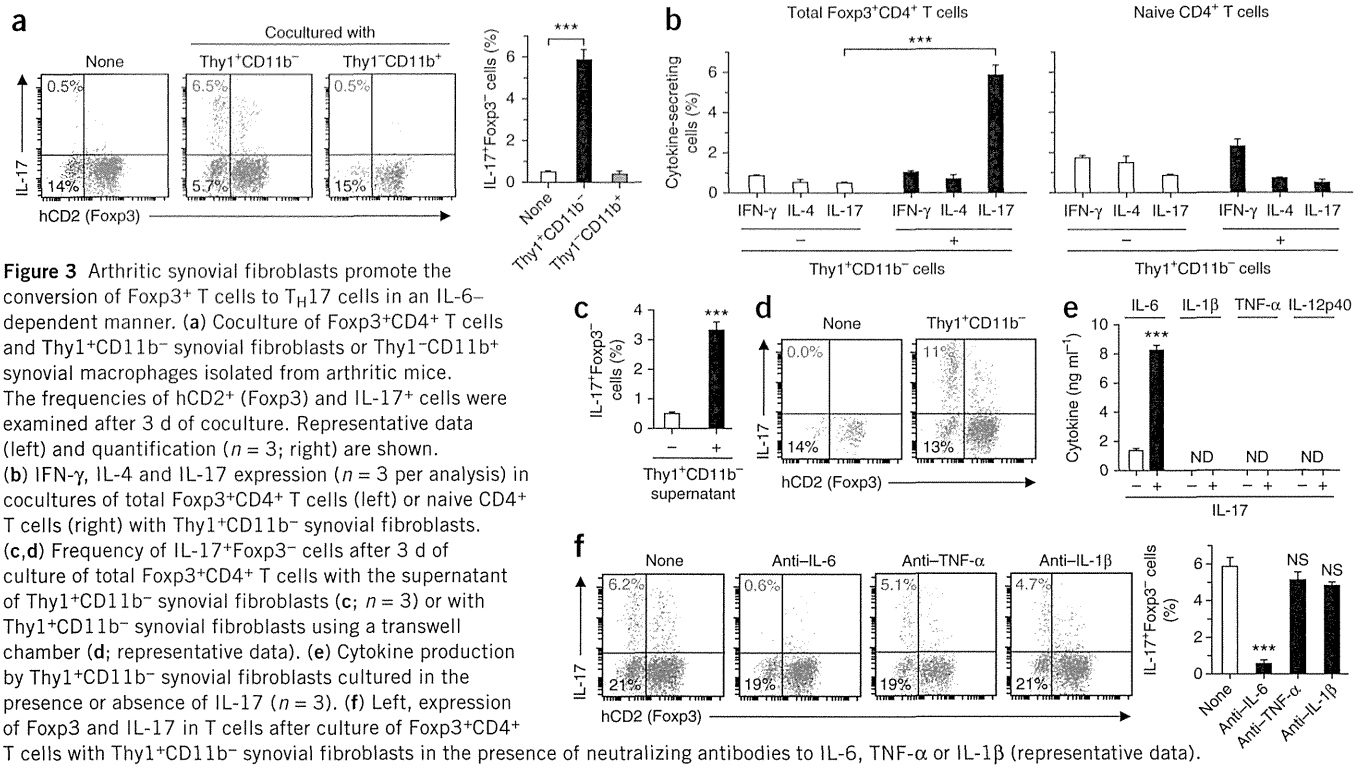

Figure 3 Arthritic synovial fibroblasts promote the conversion of Foxp3$^+$ T cells to T_H17 cells in an IL-6–dependent manner. (**a**) Coculture of Foxp3$^+$CD4$^+$ T cells and Thy1$^+$CD11b$^-$ synovial fibroblasts or Thy1$^-$CD11b$^+$ synovial macrophages isolated from arthritic mice. The frequencies of hCD2$^+$ (Foxp3) and IL-17$^+$ cells were examined after 3 d of coculture. Representative data (left) and quantification ($n = 3$; right) are shown. (**b**) IFN-γ, IL-4 and IL-17 expression ($n = 3$ per analysis) in cocultures of total Foxp3$^+$CD4$^+$ T cells (left) or naive CD4$^+$ T cells (right) with Thy1$^+$CD11b$^-$ synovial fibroblasts. (**c**,**d**) Frequency of IL-17$^+$Foxp3$^-$ cells after 3 d of culture of total Foxp3$^+$CD4$^+$ T cells with the supernatant of Thy1$^+$CD11b$^-$ synovial fibroblasts (**c**; $n = 3$) or with Thy1$^+$CD11b$^-$ synovial fibroblasts using a transwell chamber (**d**; representative data). (**e**) Cytokine production by Thy1$^+$CD11b$^-$ synovial fibroblasts cultured in the presence or absence of IL-17 ($n = 3$). (**f**) Left, expression of Foxp3 and IL-17 in T cells after culture of Foxp3$^+$CD4$^+$ T cells with Thy1$^+$CD11b$^-$ synovial fibroblasts in the presence of neutralizing antibodies to IL-6, TNF-α or IL-1β (representative data). Right, quantitative analysis of the frequency of IL-17$^+$Foxp3$^-$ cells in T cells ($n = 3$). All data are shown as the mean ± s.e.m. Statistical analyses were performed using unpaired two-tailed Student's *t* test (***$P < 0.005$; NS, not significant; ND, not detected). Data are representative of three independent experiments with triplicate culture wells.

belong to a subpopulation of pT_{reg} cells rather than tT_{reg} cells. Taken together, it is possible that exFoxp3 T cells may comprise a previously unrecognized T cell population or pT_{reg} cell–derived T cell subset that is distinct from tT_{reg} cells and activated conventional T cells. Future study of the methylation status of the *Foxp3* TSDR region in pT_{reg} cells under physiological and pathological conditions will be helpful to understand the origin of exFoxp3 T cells in more detail.

Synovial fibroblasts convert Foxp3$^+$ T cells into T_H17 cells

Accumulation of exFoxp3 T_H17 cells in arthritic joints led us to hypothesize that cells that are resident in the joint interact with Foxp3$^+$ cells, facilitating the conversion of Foxp3$^+$ T cells to T_H17 cells. To explore the role of synovial cells in the regulation of *Foxp3* stability, we isolated Thy1$^+$CD11b$^-$ cells (synovial fibroblasts) and Thy1$^-$CD11b$^+$ cells (synovial macrophages) from the joints of arthritic mice and cocultured them with total Foxp3$^+$CD4$^+$ T cells purified from unmanipulated *Foxp3*^{hCD2} mice. Coculture of Thy1$^+$CD11b$^-$ cells, but not Thy1$^-$CD11b$^+$ cells, with Foxp3$^+$CD4$^+$ cells downregulated Foxp3 expression in Foxp3$^+$CD4$^+$ T cells (**Fig. 3a**). These exFoxp3 T cells upregulate IL-17 but do not express interferon-γ (IFN-γ) or IL-4 when cocultured with arthritic synovial fibroblasts (**Fig. 3a**,**b**), suggesting that arthritic synovial fibroblasts promote the conversion of Foxp3$^+$ T cells to T_H17 cells in the joints. In contrast, when we cocultured naive CD4$^+$ T cells with Thy1$^+$CD11b$^-$ synovial fibroblasts, they did not differentiate into T_H17 cells (**Fig. 3b**). We detected IL-17$^+$Foxp3$^+$ T cells, which may appear at the transition stage during the conversion of Foxp3$^+$ T cells to T_H17 cells, in the joints and lymph nodes of arthritic mice (**Supplementary Fig. 7**), as well as in the synovium of human subjects with RA (**Supplementary Fig. 8**).

We next investigated the mechanism by which synovial fibroblasts induce the conversion of Foxp3$^+$CD4$^+$ T cells into T_H17 cells. The culture supernatant of synovial fibroblasts (**Fig. 3c**) or coculture of Foxp3$^+$CD4$^+$ T cells with transwell-separated synovial fibroblasts (**Fig. 3d**) induced conversion into T_H17 cells, indicating that cell-cell contact is not essential for conversion. We explored the soluble factors mediating this conversion by analyzing the expression of various cytokines in the supernatant (**Fig. 3e** and data not shown) and found that IL-6 was highly produced by Thy1$^+$CD11b$^-$ cells (**Fig. 3e**). The expression of IL-6 by arthritic synovial fibroblasts was further enhanced by IL-17, suggesting a potential positive feedback loop (**Fig. 3e**). A neutralizing antibody against IL-6, but neither an antibody to TNF-α nor one to IL-1β, inhibited the generation of T_H17 cells after the coculture of Foxp3$^+$CD4$^+$ T cells with synovial fibroblasts (**Fig. 3f**). These results indicate that synovial fibroblast–derived IL-6 has a crucial role in the conversion of Foxp3$^+$CD4$^+$ T cells to T_H17 cells.

exFoxp3 T_H17 cells are potent osteoclastogenic T cells

To evaluate the contribution of T_H17 cells of a Foxp3$^+$ T cell origin to the bone destruction that occurs in arthritis, we examined their ability to induce osteoclatogenesis by counting the number of osteoclasts defined by TRAP$^+$ multinucleated cells (MNCs) and the expression of RANKL, a cytokine that is essential for osteoclast differentiation[16], in comparison with both naive CD4$^+$ T cell–derived T_H17 cells and Foxp3$^+$ T cells. We found that exFoxp3 T_H17 cells had higher osteoclastogenic ability than naive CD4$^+$ T cell–derived T_H17 cells in a coculture of synovial fibroblasts and bone marrow–derived monocyte and macrophage precursor cells (BMMs) (**Fig. 4a**,**b**). Foxp3$^+$ T cells cultured in the presence of IL-2 did not have osteoclastogenic ability, which is consistent with a previous report[24]. We confirmed these findings further using *Foxp3*^{hCD2} mice crossed with IL-17–GFP knock-in mice, which enabled us to purify IL-17–expressing cells (**Supplementary Fig. 9**).

The osteoclastogenic ability of T_H17 cells has been attributed mainly to their production of IL-17, which stimulates RANKL expression in fibroblasts, as T_H17 cells alone cannot induce osteoclastogenesis despite their RANKL expression[25]. However, *Il17a*$^{-/-}$ exFoxp3 T cells that were differentiated under T_H17-polarizing conditions still induced osteoclastogenesis, suggesting a potential contribution of T cell–derived RANKL or RANKL-inducing cytokines other than IL-17A (**Fig. 4b**). We observed that exFoxp3 T_H17 cells expressed higher amounts of RANKL than did naive CD4$^+$ T cell–derived T_H17 cells (**Fig. 4c**) and coculture with synovial fibroblasts further enhanced

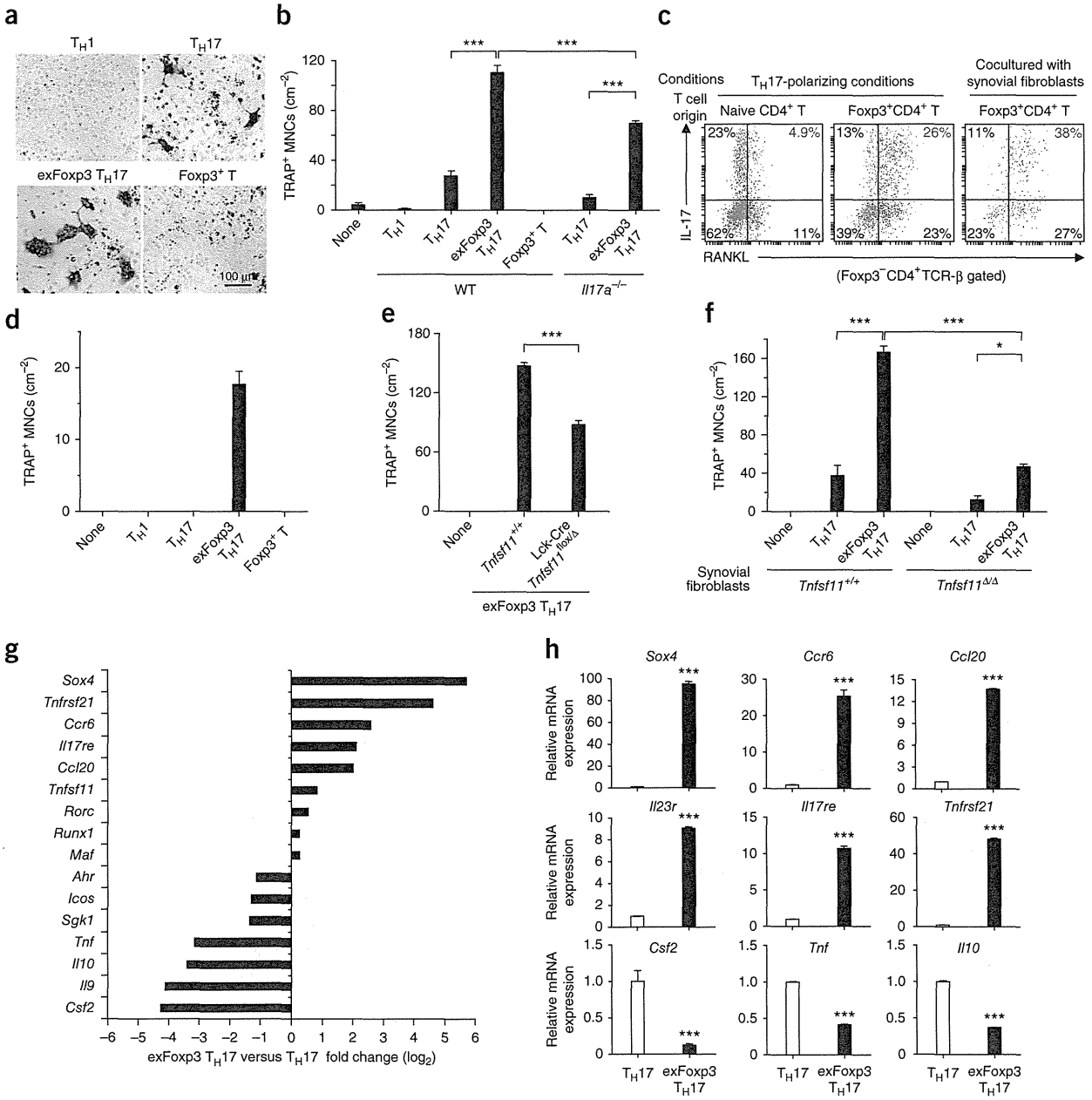

Figure 4 exFoxp3 T_H17 cells are osteoclastogenic T cells with distinct gene profiles. (**a**,**b**) Osteoclast differentiation in a coculture of BMMs, Thy1$^+$CD11b$^-$ CIA synovial fibroblasts and the T cell subsets indicated. exFoxp3 T_H17 indicates Foxp3$^-$ T cells developed from Foxp3$^+$ T cells under T_H17-polarizing conditions in this experiment. (**a**) Representative tartrate-resistant acid phosphatase (TRAP) staining. (**b**) Number of osteoclasts (TRAP$^+$ MNCs) ($n = 3$ for exFoxp3 T_H17 and Foxp3$^+$ T cells, $n = 4$ for *Il17a*$^{-/-}$ T_H17 cells, $n = 6$ for all other groups). WT, wild type. (**c**) Representative FACS profiles of RANKL and IL-17 expression in naive CD4$^+$ T cell–derived T_H17 cells (left) and exFoxp3 T_H17 cells (middle and right) that differentiated under the conditions indicated. (**d**) Number of osteoclasts (TRAP$^+$ MNCs) in a coculture of BMMs and the T cell subsets indicated ($n = 3$). (**e**,**f**) Number of osteoclasts (TRAP$^+$ MNCs) in a coculture of BMMs, synovial fibroblasts and the T cell subsets indicated. (**e**) Analysis using exFoxp3 T_H17 cells derived from *Tnfsf11*$^{+/+}$ *Foxp3*^{hCD2} or Lck-Cre *Tnfsf11*$^{flox/\Delta}$ *Foxp3*^{hCD2} mice. (**f**) Analysis using *Tnfsf11*$^{+/+}$ or *Tnfsf11*$^{\Delta/\Delta}$ arthritic synovial fibroblasts. (**g**) Microarray analysis of selected T_H17-related genes in exFoxp3 T_H17 cells and T_H17 cells. IL-17^{GFP+} *Foxp3*$^{hCD2-}$ cells developed from naive CD4$^+$ T cells or Foxp3$^+$CD4$^+$ T cells under T_H17-polarizing conditions were used as the T_H17 cells and exFoxp3 T_H17 cells, respectively. The mean fold change of three independent experiments is shown. (**h**) Quantitative RT-PCR analysis of differentially expressed genes in T_H17 cells and exFoxp3 T_H17 cells ($n = 3$). All data are representative of three independent experiments with triplicate culture wells and are shown as the mean ± s.e.m. Statistical analyses were performed using unpaired two-tailed Student's *t* test (*$P < 0.05$, ***$P < 0.005$).

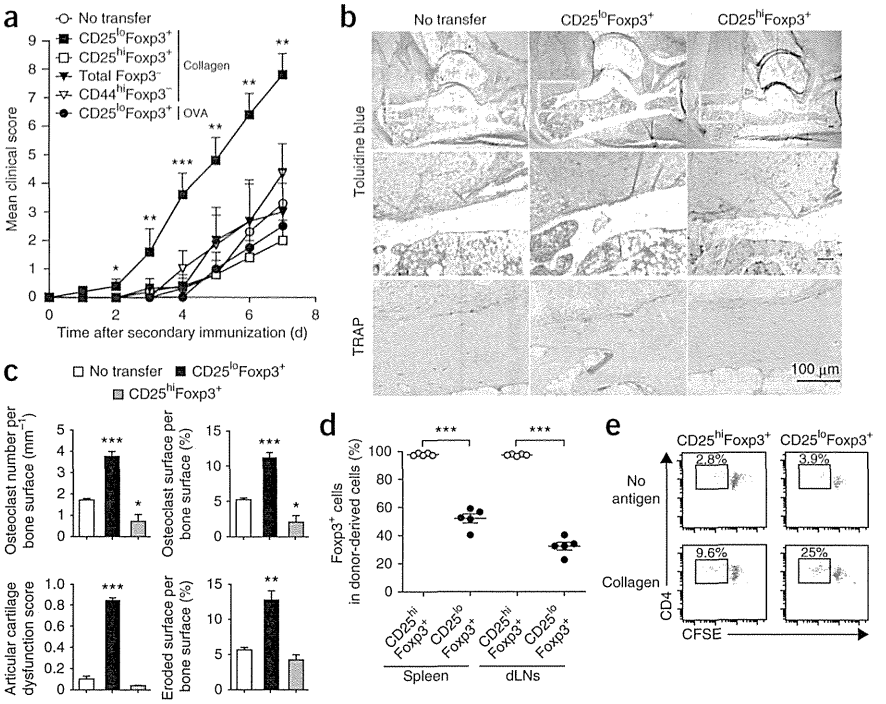

Figure 5 Pathogenic role of exFoxp3 T cells to arthritis *in vivo*. (**a**–**c**) Clinical score (**a**), histological analysis (**b**) and bone morphometric analysis (**c**) of the ankle joints of DBA/1 *Foxp3*^{hCD2} mice adoptively transferred with the indicated T cell subsets that were purified from spleens and dLNs of collagen-immunized mice ($n = 3$ for total Foxp3$^-$ cells, $n = 5$ for CD25^{lo}Foxp3$^+$ and CD25^{hi}Foxp3$^+$ cells, $n = 6$ for CD44^{hi}Foxp3$^-$ cells) or OVA-immunized mice ($n = 4$). In **b**, toluidine blue (top and middle) and TRAP (bottom) staining of ankle joints were performed. The middle row is a magnification of the boxed areas in the top row. Scale bars, 100 μm. In **c**, the quantitative bone morphometric analysis was performed using histological sections ($n = 3$). Osteoclast number per bone surface (top left), osteoclast surface per bone surface (top right), articular cartilage dysfunction score (bottom left) and eroded surface per bone surface (bottom right) are shown. (**d**) Frequency of Foxp3$^+$ cells in donor-derived CFSE$^+$CD4$^+$ T cells 1 week after secondary immunization ($n = 5$). (**e**) *In vitro* proliferative responses to type II collagen of CD25^{hi}Foxp3$^+$ or CD25^{lo}Foxp3$^+$ T cells purified from the spleens and dLNs of collagen-immunized mice. The numbers indicate the frequency of proliferating cells as determined by CFSE dilution. Representative data of more than three independent experiments are shown. All data are shown as the mean ± s.e.m. Statistical analyses were performed using one-way analysis of variance with Newman-Keuls multiple comparison test (**a**) or unpaired two-tailed Student's *t* test (**c**,**d**) (*$P < 0.05$, **$P < 0.01$, ***$P < 0.005$).

the expression of RANKL in exFoxp3 T$_H$17 cells (**Fig. 4c**). Notably, exFoxp3 T$_H$17 cells alone induced osteoclastogenesis from BMMs, even in the absence of synovial fibroblasts (**Fig. 4d**). To elucidate the relative contribution of RANKL in exFoxp3 T$_H$17 cells and synovial fibroblasts, we used exFoxp3 T$_H$17 cells from Lck-Cre *Tnfsf11* (encoding RANKL)$^{flox/\Delta}$ *Foxp3*^{hCD2} mice or *Tnfsf11*-deficient synovial fibroblasts in the T cell and synovial fibroblast coculture system. Although RANKL expressed on synovial fibroblasts has a major role in promoting osteoclastogenesis, RANKL expressed by exFoxp3 T$_H$17 cells was able to induce osteoclastogenesis, even in the absence of RANKL expression on synovial fibroblasts (**Fig. 4e,f**).

To gain molecular insight into the pathogenicity of exFoxp3 T$_H$17 cells, we performed GeneChip analysis of exFoxp3 T$_H$17 cells and naive CD4$^+$-derived T$_H$17 cells. exFoxp3 T$_H$17 cells expressed higher amounts of *Ccr6*, *Ccl20*, *Il23r*, *Il17re*, *Tnfrsf21*, *Vcam1*, *Rorc* and *Tnfsf11* but lower amounts of *Csf2*, *Tnf*, *Il10* and *Sgk1* than T$_H$17 cells (**Fig. 4g,h** and **Supplementary Fig. 10**). These data suggest that exFoxp3 T$_H$17 cells are not identical to any known pathogenic T$_H$17 cell subsets[26–29]. Notably, we found that exFoxp3 T$_H$17 cells specifically and highly express the transcription factor Sox4, which positively regulates RORγt (encoded by *Rorc*)[30] and enhances lymphoid cell survival[31]. The high expression of molecules that are involved in proliferation, such as *Pik3r3*, and the high frequency of Ki-67$^+$ cells in exFoxp3 T cells (**Supplementary Figs. 10** and **11**) suggest that under arthritic conditions, exFoxp3 T$_H$17 cells are proliferative. Thus, exFoxp3 T$_H$17 cells comprise a new pathogenic T$_H$17 cell subset that expresses Sox4, CCR6, CCL20, IL-23R, IL-17RE and RANKL.

Autoreactive CD25^{lo}Foxp3$^+$ T cells promote arthritis

Self tolerance is maintained by thymic-derived stable Foxp3$^+$CD4$^+$ T cells, which have a higher affinity for self antigens[32,33]. We hypothesized that unstable Foxp3$^+$CD4$^+$ T cells also contain self-reactive T cells and thus exert a potent arthritogenic effect after losing Foxp3 expression. To investigate the role of autoantigen-specific exFoxp3 T cells, we purified CD25^{lo}Foxp3$^+$, CD25^{hi}Foxp3$^+$, total Foxp3$^-$ and effector memory CD44^{hi}Foxp3$^-$CD4$^+$ T cells from collagen-immunized DBA/1 *Foxp3*^{hCD2} mice, which harbor collagen-specific T cells. After CFSE labeling, we transferred these cells into immunized mice 1 d before secondary immunization. Notably, CD25^{lo}Foxp3$^+$ T cells accelerated the onset and increased the severity of arthritic symptoms more than total Foxp3$^-$ or CD44^{hi}Foxp3$^-$ CD4$^+$ T cells (**Fig. 5a–c**). In contrast, the transfer of CD25^{hi}Foxp3$^+$CD4$^+$ T cells markedly inhibited osteoclast formation. More than half (50–70%) of the CD25^{lo}Foxp3$^+$ T cells lost Foxp3 expression, whereas almost all (>96%) of the CD25^{hi}Foxp3$^+$ cells retained Foxp3 expression (**Fig. 5d**). CD25^{lo}Foxp3$^+$ cells proliferated in response to type II collagen *in vitro* to a greater extent than did CD25^{hi}Foxp3$^+$ cells, suggesting that the CD25^{lo}Foxp3$^+$ cells contained a higher number of autoreactive T cells (**Fig. 5e**).

To further examine whether the exacerbation of arthritic symptoms elicited by CD25^{lo}Foxp3$^+$CD4$^+$ T cells is dependent on type II collagen–specific responses, we transferred CD25^{lo}Foxp3$^+$CD4$^+$ T cells from ovalbumin (OVA)-immunized mice to collagen-immunized mice. OVA-specific CD25^{lo}Foxp3$^+$CD4$^+$ T cells did not exacerbate arthritis scores (**Fig. 5a**). These results suggest that autoreactive pathogenic CD4$^+$ T cells were generated mainly from CD25^{lo}Foxp3$^+$CD4$^+$ T cells under arthritic conditions.

DISCUSSION

This study demonstrates that CD4$^+$ T$_H$17 cells with arthritogenic and autoreactive properties arise from Foxp3$^+$CD4$^+$ T cells, thus establishing the *in vivo* pathological importance of Foxp3$^+$CD4$^+$ T cell conversion to T$_H$17 cells. The pathogenic function of IL-17$^+$ exFoxp3 T cells may be enhanced by their higher affinity to self antigens, as well as their ability to accumulate and proliferate in inflamed tissues and stimulate

osteoclastogenesis. Conversion of Foxp3$^+$CD4$^+$ T cells into T_H17 cells in the periphery was promoted by arthritic synovial fibroblasts, thereby uncovering a new interaction of immune and tissue-resident mesenchymal cells in the breakdown of self tolerance. We propose that the fate of plastic Foxp3$^+$ T cells is a critical determinant of self tolerance versus autoimmunity. The balance between IL-2 and IL-6 regulates the development of T_{reg} and T_H17 cells from naive CD4$^+$ T cells[34], but the fate of plastic Foxp3$^+$ T cells may also be determined by this cytokine balance[35] (**Supplementary Fig. 12**). Blockade of IL-6 signaling increases the ratio of Foxp3$^+$ to T_H17 cells in the course of RA treatment[36], suggesting that some of the beneficial effects of these therapies may derive from regulation of the plasticity of Foxp3$^+$ T cell fate. Blockade of TNF-α also increases the ratio of T_{reg} to T_H17 cells[37,38], and it was recently reported that this effect is attributable to the recovery of T_{reg} cell function[38]. These reports suggest that regulating the balance of T_{reg} to T_H17 cells is important for the treatment of RA. Several RA-associated genes[39], including *Ptpn22*, *Ccr6* and *Tnfrsf14*, are highly expressed in exFoxp3 T_H17 cells (**Supplementary Fig. 13**), and we observed IL-17$^+$Foxp3$^+$ T cells in subjects with active RA (**Supplementary Fig. 8**), suggesting the potential role of exFoxp3 T_H17 cells in the pathogenesis of RA. Notably, we found that exFoxp3 T_H17 cells specifically express a set of surface molecules that may be useful in identifying arthritogenic T cells and may contribute to future diagnostic and therapeutic strategies for RA (**Supplementary Fig. 10d**). The presence of exFoxp3 T_H17 cells may be used as a biomarker for RA and be useful for predicting responsiveness to anti–IL-6 therapy. Further characterization of the mechanisms underlying the conversion and function of plastic Foxp3$^+$ T cells will provide new insights into the maintenance and restoration of self tolerance, and this will in turn lead to the development of new therapeutic strategies for autoimmune diseases.

METHODS

Methods and any associated references are available in the online version of the paper.

Accession codes. Microarray data have been deposited in the Gene Expression Omnibus database with accession code GSE48428.

Note: Any Supplementary Information and Source Data files are available in the online version of the paper.

ACKNOWLEDGMENTS

We are grateful to S. Hori (RIKEN Center for Integrative Medical Sciences) and Y. Iwakura (Tokyo University of Science) for providing B6.*Foxp3*^{hCD2} knock-in mice and *Il17a*$^{-/-}$ mice, respectively. We also thank T. Negishi-Koga, M. Shinohara, A. Terashima, M. Guerrini, L. Danks, M. Hayashi, T. Ando, Y. Ogiwara, N. Otsuka, T. Kato, C. Tsuda, T. Suda, A. Suematsu, S. Fukuse, Y. Wada, A. Izumi and K. Kaneki for discussion and assistance. This work was supported in part by a grant for the ERATO Takayanagi Osteonetwork Project from JST; a Grant-in-Aid for Challenging Exploratory Research from the Japan Society for the Promotion of Science (JSPS); a Grant-in-Aid for JSPS Fellows; and a grant for the GCOE Program from the Ministry of Education, Culture, Sports, Science and Technology of Japan. N.K. was supported by JSPS Research Fellowships for Young Scientists.

AUTHOR CONTRIBUTIONS

N.K. designed and performed experiments, interpreted the results and prepared the manuscript. K.O., S.S., T.N. and M.O. contributed to study design and manuscript preparation. T.K. contributed to microarray analysis. S.T. contributed to the analysis of human RA and osteoarthritis samples. J.A.B. generated Foxp3-GFP-Cre mice and contributed to study design and data interpretation. H.T. directed the project and wrote the manuscript.

COMPETING FINANCIAL INTERESTS

The authors declare no competing financial interests.

1. Sakaguchi, S. Naturally arising CD4$^+$ regulatory T cells for immunologic self-tolerance and negative control of immune responses. *Annu. Rev. Immunol.* **22**, 531–562 (2004).
2. Hori, S., Nomura, T. & Sakaguchi, S. Control of regulatory T cell development by the transcription factor Foxp3. *Science* **299**, 1057–1061 (2003).
3. Fontenot, J.D., Gavin, M.A. & Rudensky, A.Y. Foxp3 programs the development and function of CD4$^+$CD25$^+$ regulatory T cells. *Nat. Immunol.* **4**, 330–336 (2003).
4. Khattri, R., Cox, T., Yasayko, S.A. & Ramsdell, F. An essential role for Scurfin in CD4$^+$CD25$^+$ T regulatory cells. *Nat. Immunol.* **4**, 337–342 (2003).
5. Wan, Y.Y. & Flavell, R.A. Regulatory T-cell functions are subverted and converted owing to attenuated Foxp3 expression. *Nature* **445**, 766–770 (2007).
6. Kim, J.M., Rasmussen, J.P. & Rudensky, A.Y. Regulatory T cells prevent catastrophic autoimmunity throughout the lifespan of mice. *Nat. Immunol.* **8**, 191–197 (2007).
7. Zhou, X. *et al.* Instability of the transcription factor Foxp3 leads to the generation of pathogenic memory T cells *in vivo*. *Nat. Immunol.* **10**, 1000–1007 (2009).
8. Yang, X.O. *et al.* Molecular antagonism and plasticity of regulatory and inflammatory T cell programs. *Immunity* **29**, 44–56 (2008).
9. Oldenhove, G. *et al.* Decrease of Foxp3$^+$ T_{reg} cell number and acquisition of effector cell phenotype during lethal infection. *Immunity* **31**, 772–786 (2009).
10. Rubtsov, Y.P. *et al.* Stability of the regulatory T cell lineage *in vivo*. *Science* **329**, 1667–1671 (2010).
11. Miyao, T. *et al.* Plasticity of Foxp3$^+$ T cells reflects promiscuous Foxp3 expression in conventional T cells but not reprogramming of regulatory T cells. *Immunity* **36**, 262–275 (2012).
12. Komatsu, N. *et al.* Heterogeneity of natural Foxp3$^+$ T cells: a committed regulatory T-cell lineage and an uncommitted minor population retaining plasticity. *Proc. Natl. Acad. Sci. USA* **106**, 1903–1908 (2009).
13. Hirota, K. *et al.* Preferential recruitment of CCR6-expressing Th17 cells to inflamed joints via CCL20 in rheumatoid arthritis and its animal model. *J. Exp. Med.* **204**, 2803–2812 (2007).
14. Murakami, M. *et al.* Local microbleeding facilitates IL-6– and IL-17–dependent arthritis in the absence of tissue antigen recognition by activated T cells. *J. Exp. Med.* **208**, 103–114 (2011).
15. Korn, T., Bettelli, E., Oukka, M. & Kuchroo, V.K. IL-17 and Th17 cells. *Annu. Rev. Immunol.* **27**, 485–517 (2009).
16. Takayanagi, H. Osteoimmunology: shared mechanisms and crosstalk between the immune and bone systems. *Nat. Rev. Immunol.* **7**, 292–304 (2007).
17. Hashimoto, M. *et al.* Complement drives Th17 cell differentiation and triggers autoimmune arthritis. *J. Exp. Med.* **207**, 1135–1143 (2010).
18. Wu, H.J. *et al.* Gut-residing segmented filamentous bacteria drive autoimmune arthritis via T helper 17 cells. *Immunity* **32**, 815–827 (2010).
19. Srinivas, S. *et al.* Cre reporter strains produced by targeted insertion of EYFP and ECFP into the ROSA26 locus. *BMC Dev. Biol.* **1**, 4 (2001).
20. Sakaguchi, S. *et al.* The plasticity and stability of regulatory T cells. *Nat. Rev. Immunol.* **13**, 461–467 (2013).
21. Wehrens, E.J., Prakken, B.J. & van Wijk, F. T cells out of control—impaired immune regulation in the inflamed joint. *Nat. Rev. Rheumatol.* **9**, 34–42 (2013).
22. Ohkura, N. *et al.* T cell receptor stimulation-induced epigenetic changes and Foxp3 expression are independent and complementary events required for T_{reg} cell development. *Immunity* **37**, 785–799 (2012).
23. Feuerer, M. *et al.* Genomic definition of multiple *ex vivo* regulatory T cell subphenotypes. *Proc. Natl. Acad. Sci. USA* **107**, 5919–5924 (2010).
24. Zaiss, M.M. *et al.* T_{reg} cells suppress osteoclast formation: a new link between the immune system and bone. *Arthritis Rheum.* **56**, 4104–4112 (2007).
25. Sato, K. *et al.* Th17 functions as an osteoclastogenic helper T cell subset that links T cell activation and bone destruction. *J. Exp. Med.* **203**, 2673–2682 (2006).
26. Ghoreschi, K. *et al.* Generation of pathogenic T_H17 cells in the absence of TGF-β signalling. *Nature* **467**, 967–971 (2010).
27. Lee, Y. *et al.* Induction and molecular signature of pathogenic T_H17 cells. *Nat. Immunol.* **13**, 991–999 (2012).
28. Wu, C. *et al.* Induction of pathogenic T_H17 cells by inducible salt-sensing kinase SGK1. *Nature* **496**, 513–517 (2013).
29. Kleinewietfeld, M. *et al.* Sodium chloride drives autoimmune disease by the induction of pathogenic T_H17 cells. *Nature* **496**, 518–522 (2013).
30. Malhotra, N. *et al.* A network of high-mobility group box transcription factors programs innate interleukin-17 production. *Immunity* **38**, 681–693 (2013).
31. Ramezani-Rad, P. *et al.* SOX4 enables oncogenic survival signals in acute lymphoblastic leukemia. *Blood* **121**, 148–155 (2013).
32. Jordan, M.S. *et al.* Thymic selection of CD4$^+$CD25$^+$ regulatory T cells induced by an agonist self-peptide. *Nat. Immunol.* **2**, 301–306 (2001).
33. Sakaguchi, S., Powrie, F. & Ransohoff, R.M. Re-establishing immunological self-tolerance in autoimmune disease. *Nat. Med.* **18**, 54–58 (2012).
34. Yang, X.P. *et al.* Opposing regulation of the locus encoding IL-17 through direct, reciprocal actions of STAT3 and STAT5. *Nat. Immunol.* **12**, 247–254 (2011).
35. Tang, Q. *et al.* Central role of defective interleukin-2 production in the triggering of islet autoimmune destruction. *Immunity* **28**, 687–697 (2008).
36. Samson, M. *et al.* Inhibition of IL-6 function corrects Th17/T_{reg} imbalance in rheumatoid arthritis patients. *Arthritis Rheum.* **64**, 2499–2503 (2012).
37. Nadkarni, S., Mauri, C. & Ehrenstein, M.R. Anti-TNF-α therapy induces a distinct regulatory T cell population in patients with rheumatoid arthritis via TGF-β. *J. Exp. Med.* **204**, 33–39 (2007).
38. Nie, H. *et al.* Phosphorylation of FOXP3 controls regulatory T cell function and is inhibited by TNF-α in rheumatoid arthritis. *Nat. Med.* **19**, 322–328 (2013).
39. Viatte, S. *et al.* Genetics and epigenetics of rheumatoid arthritis. *Nat. Rev. Rheumatol.* **9**, 141–153 (2013).

ONLINE METHODS

Mice. Mice were kept under specific pathogen–free conditions, and all animal experiments were performed with the approval of the Institutional Review Board at the University of Tokyo. B6.SJL (CD45.1$^+$) and IL-17–GFP knock-in mice were obtained from the Jackson Laboratory and BIOCYTOGEN, respectively. *Foxp3*^{hCD2} knock-in mice[11], Foxp3-GFP-Cre mice[7], ROSA26-loxP-Stop-loxP-YFP reporter mice[19], *Il17a*$^{-/-}$ mice[40] mice and *Tnfsf11*$^{flox/flox}$ mice[41] were described previously. 8- to 12-week-old sex-matched mice were used for experiments unless otherwise mentioned.

Analysis of T cells in the synovium of subjects with RA or osteoarthritis. Human synovial tissue specimens were obtained from subjects undergoing joint replacement surgery or synovectomy at the Tokyo University Hospital. All the subjects with RA fulfilled the 2010 American College of Rheumatology–European League Against Rheumatism criteria for the classification of RA and provided written informed consent. This study was approved by the Institutional Review Board at The University of Tokyo. The tissue was digested with type II collagenase (1 mg ml^{-1}; Worthington) for 2 h at 37 °C. After being filtered, cells were stimulated with phorbol myristate acetate and ionomycin for 5 h. After fixation, cells were examined for the expression of Foxp3, IL-17, CD3 and CD4. Synovitis activity was evaluated macroscopically by the redness and proliferative status of the synovium membrane.

Induction of CIA. We performed CIA in 8- to 12-week-old male C57BL/6J and DBA/1J mice. Mice were immunized with an emulsion consisting of 50 µl of chicken type II collagen (Sigma-Aldrich; 4 mg ml^{-1}) and 50 µl of adjuvant given intradermally into the base of the tail at two sites. For the DBA/1 mice, we added heat-killed *Mycobacterium tuberculosis* H37Ra (Difco Laboratories; 5.0 mg ml^{-1}) in incomplete Freund's adjuvant (Difco Laboratories). For B6 mice, we added H37Ra (3.3 mg ml^{-1}) in complete Freund's adjuvant (CFA) (Difco Laboratories). Three weeks after the primary immunization, mice were challenged with the same collagen and CFA emulsion as the primary immunization. We judged the development of arthritis in the joint using the following criteria: 0, no joint swelling; 1, swelling of one finger joint; 2, mild swelling of the wrist or ankle; or 3, severe swelling of the wrist or ankle. The scores for all fingers of forepaws and hindpaws, wrists and ankles were totaled for each mouse (with a maximum possible score of 12 for each mouse).

T cell isolation and sorting. Single-cell suspensions were obtained from peripheral LNs and the spleen. Splenic erythrocytes were eliminated with red blood cell lysis buffer (Sigma-Aldrich). To purify the peripheral CD4$^+$ T cell subpopulation obtained from *Foxp3*^{hCD2} mice, the pooled spleen and LN cells were subjected to a depletion of any adherent cells by panning with goat anti-mouse IgG Fc (Cappel, 55472, 1:200) and stained with phycoerythrin (PE)-conjugated mouse anti-human CD2 (RPA-2,10, eBiosicence, 1:100). Cells were then incubated with anti-PE microbeads (Milteny Biotech) and separated on LS columns (Milteny Biotech). The hCD2$^+$ or hCD2$^-$ cells were further stained with anti-CD4 and other monoclonal antibodies and subjected to FACS sorting using FACSAriaIII (BD Biosciences). The purity of the sorted cells was >99.9%. The sorted cells were subsequently subjected to cell culture or adoptive transfer experiments. Adoptive transfer was achieved by a tail vein injection of 5 × 10^5 cells into the collagen-immunized mice 1 d before secondary immunization. For CFSE labeling, cells were stained with 5 µM CFSE (Dojindo) diluted in 0.1% BSA at 37 °C for 10 min.

T cell differentiation *in vitro*. T cells were cultured in Iscove's modified Dulbecco's medium (Sigma-Aldrich) supplemented with 2 mM L-glutamine, 10% FBS, 50 µM 2-ME, 100 U ml^{-1} penicillin and 100 µg ml^{-1} streptomycin. The following reagents were used at the concentrations indicated: 5 µg ml^{-1} anti–IFN-γ (XMG1.2, BD Biosciences), 5 µg ml^{-1} anti–IL-4 (11B11, BD Biosciences), 10 µg ml^{-1} anti–IL-6 (MP5-20F3, eBioscience), 10 µg ml^{-1} anti–TNF-α (1F3F3D4, eBioscience), 10 µg ml^{-1} anti–IL-1β (B122, eBioscience), 10 ng ml^{-1} recombinant mouse IL-1β (rmIL-1β) (R&D Systems), 10 ng ml^{-1} rmIL-2 (R&D Systems), 100 ng ml^{-1} rmIL-6 (PeproTech), 10 ng ml^{-1} rmIL-12 (PeproTech), 10 ng ml^{-1} recombinant human transforming growth factor-β1 (rhTGF-β1) (R&D Systems) and 50 ng ml^{-1} IL-23 (R&D Systems). For T cell stimulation, the sorted T cells were stimulated beads coated with monoclonal antibodies to CD3 and CD28 (Dynal; 25 µl per 1 × 10^6 cells) for 3 d. For T_H1 cell polarization, naive CD44^{lo}CD62L^{hi}Foxp3^{hCD2-}CD4$^+$ T cells were stimulated in the presence of rmIL-12 and anti–IL-4. For T_H17 cell polarization, naive CD4$^+$ T cells were stimulated in the presence of rmIL-1β, rmIL-6, rmIL-23, rhTGF-β, anti–IFN-γ and anti–IL-4. Naive CD4$^+$ T cells stimulated in the presence of anti–IFN-γ and anti–IL-4 were used as T_H0 cells. Foxp3^{hCD2+}CD4$^+$ T cells stimulated in the presence of IL-2 were used as Foxp3$^+$ T cells. For the coculture with synovial fibroblasts, synovial cells (1 × 10^4 cells per well) were cultured for 1 d before coculture using 96-well flat-bottom plates. The sorted T cells (1 × 10^5 cells per well) and beads coated with monoclonal antibodies to CD3 and CD28 were added to the culture of synovial fibroblasts. For transwell assays, synovial fibroblasts (6 × 10^4 cells per lower well) and T cells (1.5 × 10^5 cells per upper well) were cocultured using 0.4-µm-pore 24-well transwell plates (Coster) in the presence of beads coated with monoclonal antibodies to CD3 and CD28.

Type II collagen–specific response. Titers of collagen-specific antibodies in the serum were measured by ELISA using the SBA Clonotyping System (SouthernBiotech). For the T cell proliferative response, CD25^{hi}Foxp3$^+$CD4$^+$ and CD25^{lo}Foxp3$^+$CD4$^+$ T cell populations were sorted from dLNs and spleens of collagen-immunized mice 10 d after immunization. Purified cells were labeled with CFSE and cultured (1 × 10^5 per well) in the presence of denatured type II collagen (100 µg ml^{-1}), IL-2 (10 ng ml^{-1}) and Thy1.2-depleted, mitomycin C (Sigma-Aldrich)-treated splenocytes (4 × 10^5 per well) using 96-well U-bottom plates for 3 d.

Preparation of arthritic synovial fibroblasts. Synovial tissues from the ankles of mice with CIA were minced and digested by type II collagenase (1 mg ml^{-1}; Worthington) in DMEM (Sigma-Aldrich) for 2 h and then cultured in DMEM containing 20% FBS. To prepare *Tnfsf11*$^{Δ/Δ}$ arthritic synovial fibroblasts, *Tnfsf11*$^{Δ/Δ}$ mice were administered 2 mg of antibody to type II collagen (Chondrex) intravenously on day 0 and 50 µg of lipopolysaccharide intraperitoneally on day 3. Cultured fibroblasts during the fourth to seventh passages were used for the experiments. Thy1$^+$CD11b$^-$ synovial fibroblasts and Thy1$^-$CD11b$^+$ synovial macrophages were sorted by FACSAriaIII.

Flow cytometry. Antibodies conjugated with biotin, FITC, Alexa Fluor 488, PE, PerCP-Cy5.5, allophycocyanin (APC), Alexa Fluor 647, eFluor 450 or V500 were used at a 1:100 dilution unless otherwise mentioned. The following monoclonal antibodies were purchased from eBioscience: anti-human CD2 (RPA-2,10), CD3 (OKT3), CD4 (OKT4), FOXP3 (236A/E7), IL-17A (eBio64DEC17), anti-mouse CD3ε (145-2C11), CD4 (RM4-5), CD11b (also called ITGAM) (M1/70), CD25 (PC61), CD39 (24DMS1), CD44 (IM7), CD45.1 (also called PTPRC) (A20), CD45.2 (104), CD62L (also called SELL) (MEL-14), CD90.2 (also called THY1) (53-2.1), CD103 (2E7), OX40 (also called CD134) (OX-86), GITR (also called CD357) (DTA-1, 1:1600), T cell receptor-β (TCR-β) (H57-597), CCR6 (140706), RANKL (IK22/5), KLRG1 (2F1), FR4 (eBio12A5, 1:400), Foxp3 (FJK-16s), CTLA-4 (UC10-4B9), Ki-67 (B56), IFN-γ (XMG1.2), IL-4 (11B11) and IL-17A (eBio17B7). Anti-Helios (22F6) was purchased from BioLegend. Goat anti-mouse/rat Nrp1(FAB566N, 1:40) was purchased from R&D Systems. For intracellular Foxp3 staining, the Foxp3 Staining Buffer Set (eBioscience) was used. For intracellular cytokine staining, cells were stimulated with 50 ng ml^{-1} phorbol myristate acetate (Sigma-Aldrich), 500 ng ml^{-1} ionomycin (Sigma-Aldrich) and GolgiPlug (BD Biosciences) for 5 h. After washing, cells were stained for surface antigens, fixed with 4% paraformaldehyde (Nacalai Tesque) for 10 min at room temperature, permeabilized and stained with monoclonal antibodies to cytokine diluted in Perm/Wash Buffer (BD Biosciences). For the measurement of cytokine concentration in the culture supernatants, BD Cytometric Bead Array was performed. Flow cytometric analysis was performed by FACSCanto II with Diva software (BD Biosciences).

CpG methylation analysis by bisulfite sequencing. After sodium bisulfite treatment (MethylEasy Xceed, Human Genetic Signatures) of genomic DNA, modified DNA was amplified by PCR and subcloned into pUC118 Hinc 2/ BAP (Takara). PCR primers for the *Foxp3* intron 1, *Ctla4* exon 2 and *Il2ra* intron 1a regions were described previously[22].

***In vitro* assay of osteoclast differentiation.** Primary bone marrow cells were suspended in culture medium (α-MEM containing 10% FBS) supplemented with 10 ng ml^{-1} macrophage colony-stimulating factor (M-CSF) (R&D Systems) for 2 d to obtain BMMs. For a coculture of BMMs and T cells, BMMs (5×10^4 cells per well) were cultured with sorted T cells (1×10^5 cells per well) in the presence of 10 ng ml^{-1} M-CSF and beads coated with monoclonal antibodies to CD3 and CD28 for 7 d using a 96-well flat-bottom plate, and TRAP$^+$ MNCs (more than three nuclei) were counted. For a coculture of BMMs, synovial fibroblasts and T cells, BMMs (5×10^4 per well) and sorted T cells (1×10^5 or 5×10^4 cells per well) were cocultured with synovial fibroblasts (1×10^3 per well), which were isolated and cultured 1 d before coculture. Coculture was performed in the presence of beads coated with monoclonal antibodies to CD3 and CD28. After 5 d, TRAP$^+$ MNCs were counted.

Analysis of bone phenotype. The histomorphometric analysis has been described previously[41]. The articular cartilage dysfunction score was calculated by the ratio of the toluidine blue–negative area to the total articular cartilage area. For the microcomputed tomography analysis, calcaneus in the ankle joints of arthritic mice 5 weeks after secondary immunization was subjected to three-dimensional microcomputed tomography. Computed tomography scanning was performed using a ScanXmate-A100S Scanner (Comscantechno). Three-dimensional microstructural image data were reconstructed, and structural indices were calculated using TRI/3D-BON software (RATOC).

GeneChip analysis. The GeneChip analysis was performed as described previously[42]. IL-17^{GFP+}Foxp3^{hCD2-} cells differentiated from Foxp3^{hCD2+}CD4$^+$ cells under T_H17-polarizing conditions for 4 d were sorted and used as exFoxp3 T_H17 cells. IL-17^{GFP+}Foxp3^{hCD2-} cells differentiated from naive CD4$^+$ cells under T_H17-polarizing conditions were used as T_H17 cells. IL-17^{GFP-}Foxp3^{hCD2+} cells after the culture of Foxp3^{hCD2+}CD4$^+$ cells in the presence of IL-2 were used as T_{reg} cells. T_H0 cells were also used for this analysis. $8–10 \times 10^5$ cells of each T cell subset after culture were subsequently subjected to RNA extraction. The total RNAs extracted from these cells were used for cDNA synthesis by reverse transcription, followed by synthesis of biotinylated cRNA through *in vitro* transcription. After cRNA fragmentation, hybridization with the Mouse Genome 430 2.0 Array (Affymetrix) was performed as described previously[42]. The main part of the data set was deposited and can be obtained from the Genome Network Platform (http://genomenetwork.nig.ac.jp/). We performed microarray analysis using three sets of T cell samples that were independently prepared from 16–18 IL-17^{GFP} *Foxp3*^{hCD2} mice (51 mice in total). The microarray data have been deposited in the Gene Expression Omnibus database with accession code GSE48428.

Statistical analyses. Statistical analyses were performed using one-way analysis of variance with Newman-Keuls multiple comparison test and unpaired two-tailed Student's *t* test ($^*P < 0.05$, $^{**}P < 0.01$, $^{***}P < 0.005$; NS, not significant; ND, not detected in all figures). All data are expressed as the mean ± s.e.m. The results are representative examples of more than three independent experiments. We estimated the sample size considering the variation and mean of the samples. We tried to reach the conclusion using as small a size of samples as possible. We usually excluded samples if we observed any abnormality in terms of size, weight or apparent disease symptoms in mice before performing experiments. However, we did not exclude animals here, as we did not observe any abnormalities in the present study. Neither randomization nor blinding was done in this study. Statistical tests are justified as appropriate for every figure, and the data meet the assumptions of the tests.

40. Nakae, S. *et al.* Antigen-specific T cell sensitization is impaired in IL-17–deficient mice, causing suppression of allergic cellular and humoral responses. *Immunity* **17**, 375–387 (2002).
41. Nakashima, T. *et al.* Evidence for osteocyte regulation of bone homeostasis through RANKL expression. *Nat. Med.* **17**, 1231–1234 (2011).
42. Takayanagi, H. *et al.* Induction and activation of the transcription factor NFATc1 (NFAT2) integrate RANKL signaling in terminal differentiation of osteoclasts. *Dev. Cell* **3**, 889–901 (2002).

Biomaterials 35 (2014) 6677–6686

Contents lists available at ScienceDirect

Biomaterials

journal homepage: www.elsevier.com/locate/biomaterials

Poly(2-methacryloyloxyethyl phosphorylcholine) grafting and vitamin E blending for high wear resistance and oxidative stability of orthopedic bearings

Masayuki Kyomoto [a,b,d], Toru Moro [b,c], Shihori Yamane [a,b,d], Kenichi Watanabe [b,d], Masami Hashimoto [e], Yoshio Takatori [b,c], Sakae Tanaka [c], Kazuhiko Ishihara [a,*]

[a] Department of Materials Engineering, School of Engineering, The University of Tokyo, 7-3-1 Hongo, Bunkyo-ku, Tokyo 113-8656, Japan
[b] Division of Science for Joint Reconstruction, Graduate School of Medicine, The University of Tokyo, 7-3-1 Hongo, Bunkyo-ku, Tokyo 113-8655, Japan
[c] Sensory & Motor System Medicine, Faculty of Medicine, The University of Tokyo, 7-3-1 Hongo, Bunkyo-ku, Tokyo 113-8655, Japan
[d] Research Department, KYOCERA Medical Corporation, 3-3-31 Miyahara, Yodogawa-ku, Osaka 532-0003, Japan
[e] Materials Research and Development Laboratory, Japan Fine Ceramics Center, 2-4-1 Mutsuno, Atsuta-ku, Nagoya 456-8587, Japan

ARTICLE INFO

Article history:
Received 14 March 2014
Accepted 12 April 2014
Available online 15 May 2014

Keywords:
Joint replacement
Polyethylene
Phosphorylcholine
Antioxidant
Wear mechanism
Oxidation

ABSTRACT

The ultimate goal in manipulating the surface and substrate of a cross-linked polyethylene (CLPE) liner is to obtain not only high wear resistance but also high oxidative stability and high-mechanical properties for life-long orthopedic bearings. We have demonstrated the fabrication of highly hydrophilic and lubricious poly(2-methacryloyloxyethyl phosphorylcholine) (PMPC) grafting layer onto the antioxidant vitamin E-blended CLPE (HD-CLPE(VE)) surface. The PMPC grafting layer with a thickness of 100 nm was successfully fabricated on the vitamin E-blended CLPE surface by using photoinduced-radical graft polymerization. Since PMPC has a highly hydrophilic nature, the water wettability and lubricity of the PMPC-grafted CLPE and HD-CLPE(VE) surfaces were greater than that of the untreated CLPE surface. The PMPC grafting contributed significantly to wear reduction in a hip-joint simulator wear test. Despite high-dose gamma-ray irradiation for cross-linking and further UV irradiation for PMPC grafting, the substrate modified by vitamin E blending maintained high-oxidative stability because vitamin E is an extremely efficient radical scavenger. Furthermore, the mechanical properties of the substrate remained almost unchanged even after PMPC grafting or vitamin E blending, or both PMPC grafting and vitamin E blending. In conclusion, the PMPC-grafted HD-CLPE(VE) provided simultaneously high-wear resistance, oxidative stability, and mechanical properties.

1. Introduction

Over the last half century, total hip arthroplasty (THA) has been one of the most successful joint surgeries for osteoarthritis and rheumatoid arthritis. Most patients experience dramatic pain relief, increased daily activity, and restored quality of life after THA. Owing to the aging global population, the number of primary and revised THAs performed has increased significantly year on year [1]. However, the incidence of osteolysis that leads to aseptic loosening greatly limits the duration and clinical outcome of this type of surgery [2,3]. Osteolysis is triggered by a host inflammatory response to wear particles produced at the bearing interface of the artificial joint. A typical device consists of an ultra-high molecular weight polyethylene (PE; currently cross-linked PE or CLPE) acetabular liner and a cobalt–chromium–molybdenum (Co–Cr–Mo) alloy femoral head, particles of which undergo phagocytosis by macrophages and induce the secretion of bone-resorptive cytokines [4]. Therefore, the reduction of the wear particles has become an important issue and the increasing focus of many studies.

To reduce wear, we have recently developed an articular-cartilage-inspired technology for surface modification with poly (2-methacryloyloxyethyl phosphorylcholine) (PMPC) grafting to develop a life-long acetabular liner in an artificial hip replacement [5–10]. Modification of the bearing surfaces of an artificial joint with a hydrophilic layer should increase lubrication to levels that match articular cartilage under physiological conditions. The synthetic molecule 2-methacryloyloxyethyl phosphorylcholine (MPC) is commonly used to prepare highly hydrophilic and antibiofouling

* Corresponding author. Tel.: +81 3 5841 7124; fax: +81 3 5841 8647.
E-mail address: ishihara@mpc.t.u-tokyo.ac.jp (K. Ishihara).

http://dx.doi.org/10.1016/j.biomaterials.2014.04.051
0142-9612/

polymer biomaterials [11–14]. MPC polymers have great potential for applications in the fields of biomedical science and bioengineering because they possess beneficial properties such as excellent antibiofouling ability and suppression of friction. Thus, a number of medical devices, including intravascular stents [12], soft contact lenses [13], artificial hearts [14], and artificial hip joints [9], have been developed from MPC polymers and applied clinically. The biomedical efficacy and safety of MPC polymers are therefore well established. A nanometer-scale layer of PMPC was formed on a CLPE surface to recreate the ideal hydrophilicity and lubricity of a physiological joint surface [15–17]. In the present study, the PMPC grafting was accomplished using a photoinduced- (i.e., through ultraviolet (UV) irradiation) radical polymerization technique [18–20].

However, lubrication is only one of several important indicators of the clinical performance of acetabular liners. Oxidation degradation of the first generation of CLPE by gamma-ray sterilization has been regarded as a potential limiting factor for the longevity of artificial hip replacements [21,22]. During gamma-ray irradiation, free radicals are formed in the PE molecular structure through cleavage of molecular bonding, and most of these free radicals are recombined in the cross-linking in the amorphous phase of PE. However, the free radicals in the crystalline phase of PE are long-lived and cause embrittlement through a cascading oxidation reaction [21]. Hence, other important indicators of acetabular liner performance include oxidation, which simultaneously preserves the mechanical properties of CLPE. The incorporation of the antioxidant vitamin E (α-tocopherol) has been proposed recently as an alternative to post-irradiation melting treatment after gamma-ray irradiation to avoid oxidation [23]. Vitamin E is a free-radical scavenger and a well-established biological antioxidant. It is a naturally occurring compound whose function as an additive is to react with free radicals in the cell membrane and prevent oxidation-induced degradation of the polyunsaturated fatty acid. Most frequently, vitamin E is incorporated in PE by blending it into PE powder before consolidation to form a molded bar or sheet stock, and subsequent gamma-ray irradiation is carried out for cross-linking. In this process, the vitamin E concentration and irradiation dose are relatively easy to control and can be optimized.

In the study reported here, we prepared a highly hydrophilic and lubricious nanometer-scale surface by grafting a PMPC layer onto the surface of an antioxidative CLPE substrate that was modified by vitamin E blending. Our ultimate goal in manipulating the surface and substrate of the CLPE liner was not just to obtain high wear resistance, but also high oxidative stability and excellent mechanical properties for life-long orthopedic bearings. The presence of vitamin E in the substrate prevented degradation caused by oxidation, but it could also reduce the efficiency of cross-linking and PMPC grafting while the vitamin E itself reacted [24]. Therefore, the modification process for the substrate (i.e., vitamin E blending) and surface (i.e., PMPC grafting) must be optimized to simultaneously obtain wear resistance, oxidative stability, and excellent mechanical properties for life-long orthopedic bearings. We investigated the effects of PMPC grafting and vitamin E blending on these three properties of liners for artificial hip joints; such investigations are of great importance in the design of life-long artificial joints and to better understand how the use of this material can affect the longevity of artificial hip joints.

In the course of the study, we searched for answers to three questions: (1) Is it possible to prepare the PMPC grafting layer on the CLPE surface, regardless of the presence of vitamin E? (2) Will the hydration lubrication characteristics of the PMPC grafting layer affect wear resistance? (3) Will vitamin E provide oxidative stability despite the high-dose gamma-ray irradiation for cross-linking and further UV irradiation for PMPC grafting?

2. Materials and methods

2.1. Chemicals

Benzophenone and acetone were purchased from Wako Pure Chemical Industries, Ltd. (Osaka, Japan). Industrially synthesized MPC was supplied by NOF Corp. (Tokyo, Japan) [25]. A compression-molded bar stock of 0.1 mass% vitamin E-blended polyethylene (PE(VE); GUR1020E resin, Orthoplastics Ltd., Lancashire, UK) was irradiated with a high dose (HD; 100 kGy) of gamma-rays in a N_2 gas atmosphere and annealed at 120 °C for 12 h in N_2 gas in order to facilitate cross-linking. Hereafter, this polyethylene material is referred to as HD-CLPE(VE). As the control, a compression-molded bar stock of polyethylene without any additives (GUR1020 resin, Orthoplastics Ltd.) was irradiated with a 50 kGy dose of gamma-rays in a N_2 gas atmosphere, and annealed at 120 °C for 7.5 h in N_2 gas to facilitate cross-linking. Hereafter, this polyethylene material is referred to as CLPE. Samples of CLPE and HD-CLPE(VE) were then machined from the bar stocks after cooling, washed with aqueous polysorbate-surfactant solutions and ethanol, and dried at room temperature.

2.2. PMPC grafting on CLPE

The CLPE and HD-CLPE(VE) samples were immersed for 30 s in acetone containing 10 mg/mL benzophenone, and then dried in the dark at room temperature to remove the acetone. MPC was dissolved in degassed pure water to a concentration of 0.5 mol/L [17]. The benzophenone-coated CLPE and HD-CLPE(VE) samples were then immersed in the aqueous MPC solution. Photoinduced-radical graft polymerization was carried out on the CLPE and HD-CLPE(VE) surfaces using UV irradiation (UVL-400HA ultra-high pressure mercury lamp, Riko-Kagaku Sangyo Co., Ltd., Funabashi, Japan) with an intensity of 5 mW/cm^2 at 60 °C for 90 min; a filter (model D-35, Toshiba Corp., Tokyo, Japan) was used to permit the passage of only UV light with a wavelength of 350 ± 50 nm [8,19,20]. After the polymerization, the PMPC-grafted CLPE and PMPC-grafted HD-CLPE(VE) samples were removed, washed with pure water and ethanol, and dried at room temperature.

2.3. Surface chemical analysis

The elemental surface conditions of the PMPC-grafted CLPE and PMPC-grafted HD-CLPE(VE) samples were analyzed by X-ray photoelectron spectroscopy (XPS). The XPS spectra were obtained using an XPS spectrophotometer (AXIS-HSi165, Kratos/Shimadzu Co., Kyoto, Japan) equipped with a 15 kV Mg-Kα radiation source at the anode. The take-off angle of the photoelectrons was maintained at 90°. The functional group vibrations of the PMPC-grafted CLPE and PMPC-grafted HD-CLPE(VE) samples were examined by Fourier-transform infrared (FT-IR) spectroscopy with attenuated total reflection (ATR) equipment. The FT-IR/ATR spectra were obtained using an FT-IR analyzer (FT/IR615; JASCO Co., Ltd., Tokyo, Japan) for 32 scans over the 800–2000 cm^{-1} range at a resolution of 4.0 cm^{-1}.

2.4. Cross-sectional observations by transmission electron microscopy

Cross-sections of the PMPC-grafted CLPE and HD-CLPE(VE) samples were observed using transmission electron microscopy (TEM). The samples were embedded in epoxy resin, stained with ruthenium oxide vapor at room temperature, and then sliced into ultra-thin films (approximately 100 nm-thick) using a Leica Ultra Cut UC microtome (Leica Microsystems, Ltd., Wetzlar, Germany). A JEM-1010 electron microscope (JEOL, Ltd., Tokyo, Japan) was used for the TEM observations at an acceleration voltage of 100 kV.

2.5. Mechanical tests

The mechanical properties of the PMPC-grafted CLPE and PMPC-grafted HD-CLPE(VE) substrates were evaluated using a series of tests. Tensile testing was performed according to ASTM D638 using type IV tensile bar specimens that measured 1.5 mm in thickness and a crosshead speed of 50.8 mm/min. Each of the PMPC-grafted CLPE and PMPC-grafted HD-CLPE(VE) samples was divided into ten specimens, and each was evaluated individually. A double-notched (notch depth = 4.57 ± 0.08 mm) Izod impact test was performed according to ASTM F648, with six specimens tested for each PMPC-grafted CLPE samples and each PMPC-grafted HD-CLPE(VE) sample. The shore hardness (D) was measured according to ASTM D2240, with five specimens tested for each PMPC-grafted CLPE sample and each PMPC-grafted HD-CLPE(VE) sample. Creep deformation was measured by applying a constant load (1130 kgf for 24 h) to a specimen and then measuring the height displacement, according to ASTM D621, with four specimens tested for each PMPC-grafted CLPE sample and each PMPC-grafted HD-CLPE(VE) sample. Each sample was sterilized by 25 kGy gamma-rays in N_2 gas. The results of each mechanical test were expressed as the mean values ± the standard deviation.

2.6. Wettability and friction tests

Static-water contact angles were measured on each of the PMPC-grafted CLPE and PMPC-grafted HD-CLPE(VE) samples by employing the sessile-drop method using an optical-bench-type contact-angle goniometer (Model DM300, Kyowa Interface Science Co., Ltd., Saitama, Japan). Drops of purified water (1 μL) were deposited on the PMPC-grafted CLPE and PMPC-grafted HD-CLPE(VE) surfaces, and

the contact angles were directly measured after 60 s using a microscope. Fifteen areas were evaluated for each sample, and the mean values ± the standard deviation were calculated.

Unidirectional friction tests were performed using a ball-on-plate machine (Tribostation 32, Shinto Scientific Co., Ltd., Tokyo, Japan). Six specimens of each of the PMPC-grafted CLPE and PMPC-grafted HD-CLPE(VE) samples were evaluated. Each specimen was sterilized by 25-kGy gamma-rays in N_2 gas. A 9-mm-diameter pin made of a Co–Cr–Mo alloy was also prepared. The surface roughness (R_a) of the pin was <0.01 μm, which was comparable to that of currently used femoral head products. The friction test was performed for each specimen at room temperature using a load of 0.98 or 4.9 N (the contact stress roughly calculated by Hertzian theory was approximately 29 or 49 MPa, respectively), a sliding distance of 25 mm, and a frequency of 1 Hz. A maximum of 100 cycles were carried out, and pure water was used for lubrication. The mean dynamic coefficients of friction were determined by averaging the values of five data points taken from the 96–100 cycles.

2.7. Hip-simulator wear test

A 12-station hip simulator (MTS Systems Corp., Eden Prairie, MN, USA) using the untreated CLPE, PMPC-grafted CLPE, and PMPC-grafted HD-CLPE(VE) liners with an inner and outer diameter of 26 and 52 mm, respectively, was used for the wear test according to ISO 14242-3. Four specimens of each of the untreated CLPE, PMPC-grafted CLPE, and PMPC-grafted HD-CLPE(VE) liners were prepared. Each liner was sterilized by 25 kGy gamma-rays in N_2 gas. A Co–Cr–Mo alloy ball measuring 26 mm in diameter (K-MAX® HH-02; KYOCERA Medical Corp., Osaka, Japan) was used as the femoral head. A mixture of 25 vol% bovine serum, 20 mmol/L ethylene diamine-*N*, *N*, *N*′, *N*′-tetraacetic acid (EDTA), and 0.1 mass% sodium azide was used as the lubricant. The lubricant was replaced every 5.0×10^5 cycles. Gait cycles were applied to simulate a physiological loading curve (Paul-type) with double peaks at 1793 and 2744 N, and multidirectional (biaxial and orbital) motion with a frequency of 1 Hz. Gravimetric wear was determined by weighing the liners at intervals of each 5.0×10^5 cycles. Load-soak controls ($n = 2$) were used to compensate for fluid absorption by the specimens, according to ISO 14242-2. Testing was continued for a total of 1.0×10^7 cycles. Because the gravimetric method was used, the weight loss of each of the tested liners was corrected by subtracting the weight gain resulting from the load-soak control. However, this correction was not considered to be perfect because only the tested liners were continuously moved and subjected to the load.

After 1.0×10^7 cycles of the hip-simulator wear test, the volumetric wear of the liners was evaluated using a three-dimensional (3D) coordinate-measurement machine (BHN-305, Mitutoyo Corp., Kawasaki, Japan). The structures were then reconstructed using 3D modeling software (Imageware, Siemens PLM Software Inc., Plano, TX, USA).

The wear particles were isolated from the bovine serum solution, which was then used as a lubricant in the hip-simulator wear test. To isolate the wear particles, the lubricant was incubated in a 5 mol/L sodium hydroxide solution for 3 h at 65 °C to digest adhesive proteins that degraded and precipitated. In order to avoid artifacts, the contaminating proteins were removed by extraction with solutions of several densities: sugar solution, 1.20 g/cm^3 and 1.05 g/cm^3; isopropyl alcohol solution, 0.98 g/cm^3 and 0.90 g/cm^3. This was followed by centrifugation at 2.55×10^4 rpm for 3 h at 5 °C (himac CP 70MX; Hitachi Koki Co., Ltd., Tokyo, Japan). The collected solution was sequentially filtered through a 0.1-μm membrane filter, and the membrane was observed under a field-emission scanning electron microscope (FE-SEM; JSM-633OF, JEOL DATUM Co., Ltd., Tokyo, Japan) at an acceleration voltage of 20 kV after gold deposition.

2.8. Oxidative stability tests

The residual free radicals of the PMPC-grafted CLPE and PMPC-grafted HD-CLPE(VE) samples, obtained before and after gamma-ray sterilization at 25 kGy in N_2, were analyzed by electron spin resonance (ESR). The ESR spectra of PMPC-grafted CLPE and PMPC-grafted HD-CLPE(VE) were obtained using an ESR spectrometer (JES-FA300, JEOL RESONANCE Inc., Akishima, Japan) in a cylindrical TE011 resonant cavity at 9.1 GHz and 25 °C. The external magnetic field was modulated at 100 kHz to detect the first-order derivative of the absorption line. The relative concentration of defects in each grain was calculated by double numerical integration of the observed absorption-derivative peaks relative to the signal of 4-hydroxy-2,2,6,6-tetramethyl-4-piperidinol-1-oxyl (Sigma–Aldrich Corp., Saint Louis, MO, USA) as a control sample. Six specimens were evaluated for each PMPC-grafted CLPE sample and each PMPC-grafted HD-CLPE(VE) sample, and the results were expressed as the mean values ± the standard deviation.

The oxidative stability (oxidative-induction time) of PMPC-grafted CLPE and PMPC-grafted HD-CLPE(VE) sterilized by 25-kGy gamma-rays in N_2 gas was evaluated by differential scanning calorimetry (DSC) with a DSC-Q100 differential scanning calorimeter (TA Instruments Inc., New Castle, DE, USA) according to ASTM D3895. Samples weighing approximately 5 mg were placed in an aluminum pan. The samples were kept at 30 °C for 5 min under a nitrogen flow of 50 mL/min, heated to 200 °C at a rate of 20 °C/min, and then held for 5 min for equilibration while the nitrogen flow was maintained. After that, the purge gas was switched to oxygen with a flow rate of 50 mL/min. The oxidative-induction time was obtained as the time between the oxygen switch and the sharp increase in heat flow resulting from the exothermic nature of the oxidation reaction. Six specimens were evaluated for each PMPC-grafted CLPE sample and each PMPC-grafted HD-CLPE(VE) sample, and the results were expressed as the mean values ± the standard deviation.

The oxidative degradation (oxidation index) of the PMPC-grafted CLPE and PMPC-grafted HD-CLPE(VE) samples that underwent accelerated aging was evaluated by microscopic FT-IR according to ASTM F2102. The PMPC-grafted CLPE and PMPC-grafted HD-CLPE(VE) samples sterilized by 25-kGy gamma-rays in N_2 gas were subjected to the conditions of accelerated aging, i.e., exposure to 80 °C in air for 21 days [26]. A thin film (thickness of 100–200 μm) of the cross-section was sliced from each of the aged samples. The FT-IR spectra were obtained using a microscopic FT-IR analyzer (Spectrum BX, Perkin–Elmer Corp., MA, USA) for 100 scans over the range of 800–2000 cm^{-1} at a resolution of 4.0 cm^{-1}. The oxidation index was defined as the ratio of the carbonyl peak area at 1720 cm^{-1} to the methylene peak area at 1360 cm^{-1}. Four films were evaluated for each sample, and the mean values ± the standard deviation were calculated.

2.9. Statistical analyses

The mean values of the three groups (untreated CLPE, PMPC-grafted CLPE, and PMPC-grafted HD-CLPE(VE)) were compared by one-factor analysis of variance (ANOVA), and the significant differences of the all comparable properties were determined by post-hoc testing using the Bonferroni method. The dynamic coefficients of friction (unidirectional friction test) of each group under loadings of 0.98 and 4.9 N were compared by using a Student's *t*-test. All the statistical analyses were performed using an add-on (Statcel 2, OMS Publishing Inc., Tokorozawa, Japan) to Microsoft Excel® 2003 (Microsoft Corp., Redmond, WA, USA).

3. Results

Vitamin E blending was found to have no effect on the extent of PMPC grafting. Fig. 1 shows the XPS and FT-IR/ATR spectra of the untreated CLPE, and PMPC-grafted CLPE, and PMPC-grafted HD-CLPE(VE). The XPS spectra of the binding energy region of the nitrogen (N) and phosphorous (P) electrons showed peaks for PMPC-grafted CLPE and PMPC-grafted HD-CLPE(VE), while these peaks were not observed in the case of untreated CLPE (Fig. 1A). The peaks at 403 and 134 eV are attributed to the trimethylammonium group and phosphate group, respectively, which indicate the presence of phosphorylcholine in the MPC units. A transmission absorption peak was observed at 1460 cm^{-1} for all samples (Fig. 1B). This peak is chiefly attributed to the methylene (CH_2) chain in the CLPE or HD-CLPE(VE) substrate, the blended vitamin E, and the grafted PMPC. However, absorption peaks at 1720, 1240, 1080, and 970 cm^{-1} were observed only in the spectra for PMPC-grafted surfaces. These peaks correspond to the carbonyl group (C=O) and the phosphate group (P–O) in the MPC unit, respectively. After PMPC grafting, peaks attributed to the MPC unit were clearly observed in both XPS and FT-IR/ATR spectra of PMPC-grafted CLPE and PMPC-grafted HD-CLPE(VE). As shown in the cross-sectional TEM images in Fig. 2, the PMPC-grafting process afforded a uniform grafted PMPC layer with an almost constant thickness of 100–150 nm on the surface of both CLPE and HD-CLPE(VE). In addition, neither cracking nor delamination was observed at the substrates and the interface between the grafted PMPC layer and the CLPE or HD-CLPE(VE) substrate. These results indicate that PMPC was successfully grafted on the CLPE and HD-CLPE(VE) surfaces [15–20].

Some mechanical properties of the untreated CLPE, PMPC-grafted CLPE, and PMPC-grafted HD-CLPE(VE) are summarized in Table 1. The tensile ultimate strength, hardness, and creep deformation properties did not differ significantly between all groups examined in this study. In contrast, the tensile yield strength differed slightly among all three groups. The elongation and impact strength in the PMPC-grafted HD-CLPE(VE) were also slightly decreased compared to those in the untreated CLPE and PMPC-grafted CLPE. However, all mechanical properties of the untreated CLPE, PMPC-grafted CLPE, and PMPC-grafted HD-CLPE(VE) met the requirements of ASTM F648 and F2695.

The PMPC grafting affected the hydration and friction kinetics of the CLPE surface, regardless of vitamin E blending. Fig. 3 shows the

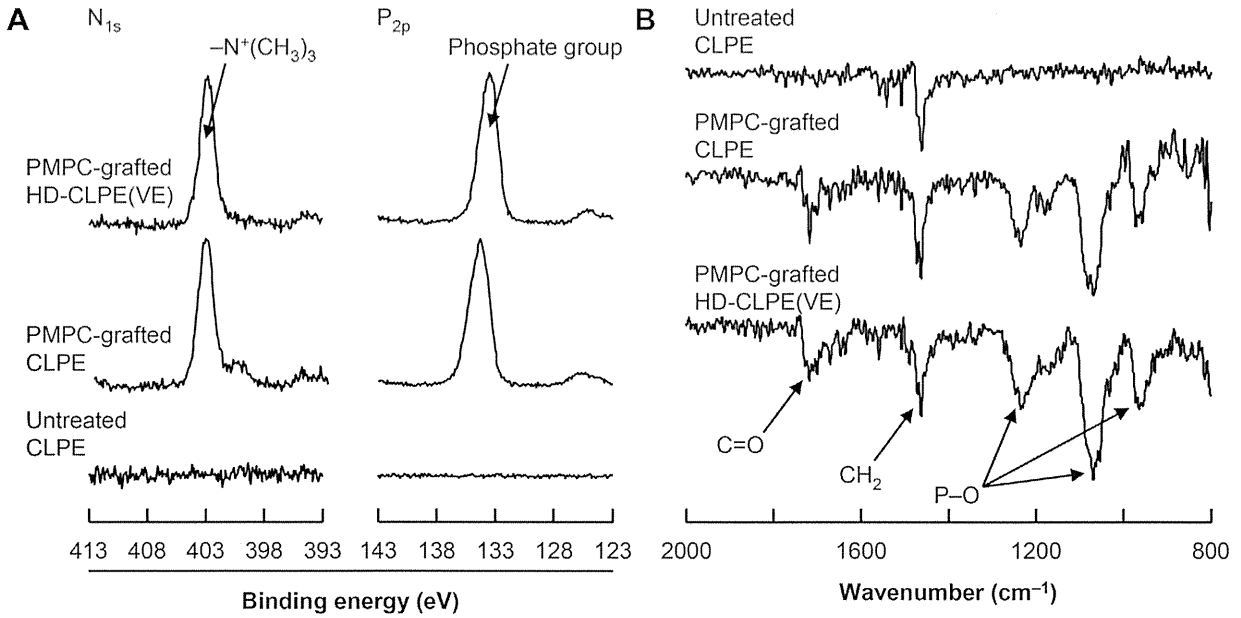

Fig. 1. (A) XPS and (B) FT-IR/ATR spectra of untreated CLPE, PMPC-grafted CLPE, and PMPC-grafted HD-CLPE(VE) samples.

static-water contact angles on the untreated CLPE, PMPC-grafted CLPE, and PMPC-grafted HD-CLPE(VE) surfaces, as well as the dynamic coefficient of friction between water and all three surfaces. The static-water contact angle on untreated CLPE was 96°, and it decreased markedly to 27° and 30°, respectively, after PMPC grafting was carried out on the CLPE and HD-CLPE(VE) surfaces (Fig. 3A). The dynamic coefficients of friction between water and PMPC-grafted CLPE and PMPC-grafted HD-CLPE(VE) decreased markedly, with the surfaces exhibiting an approximately 80–90% reduction in the coefficient compared with the untreated CLPE surface (Fig. 3B). Interestingly, the dynamic coefficients of friction of the PMPC-grafted CLPE under a 4.9 N loading decreased significantly compared to those under a 0.98 N loading, regardless of vitamin E blending.

In the hip-simulator wear test with 1.0×10^7 cycles, the characteristics of the PMPC-grafted surface affected the durability of the CLPE or HD-CLPE(VE) liner. In the absence of vitamin E blending or PMPC grafting, fluid (e.g., water, proteins, and lipids) absorption in the load-soak control liners, determined by the weight gain, was increased in a cycle-dependent manner (Fig. 4A). During the hip-simulator wear test, the PMPC grafting drastically decreased the gravimetric wear not only in the CLPE liner, but also to a similar level in the HD-CLPE(VE) liner (Fig. 4B). Furthermore, there was a slight and gradual increase in weight of the untreated CLPE, PMPC-grafted CLPE, and PMPC-grafted HD-CLPE(VE) liners during the testing period, which is partially attributed to greater fluid absorption by the tested liners than was allowed for by the load-soak controls. As noted earlier, correction using the load-soak control was not a perfect approach because only the tested liners were continuously moved and loaded. Three-dimensional coordinate measurements of the PMPC-grafted CLPE and PMPC-grafted HD-CLPE(VE) liners revealed barely detectable volumetric wear, in contrast to the substantial wear detected for the untreated CLPE liners (Fig. 5A). The volumetric wear images in Fig. 5A are in agreement with the gravimetric wear data shown in Fig. 4B. Remarkably, extremely small and barely observable wear particles were produced by the PMPC-grafted CLPE and PMPC-grafted HD-CLPE(VE) liners during the hip-simulator wear test (Fig. 5B). The wear particles of the untreated CLPE liners, and the small quantity of wear particles produced by the PMPC-grafted CLPE and PMPC-grafted HD-CLPE(VE) liners, consisted of only sub-micrometer-sized granules. The vitamin E blending and PMPC grafting did not affect the morphologies of the wear particles.

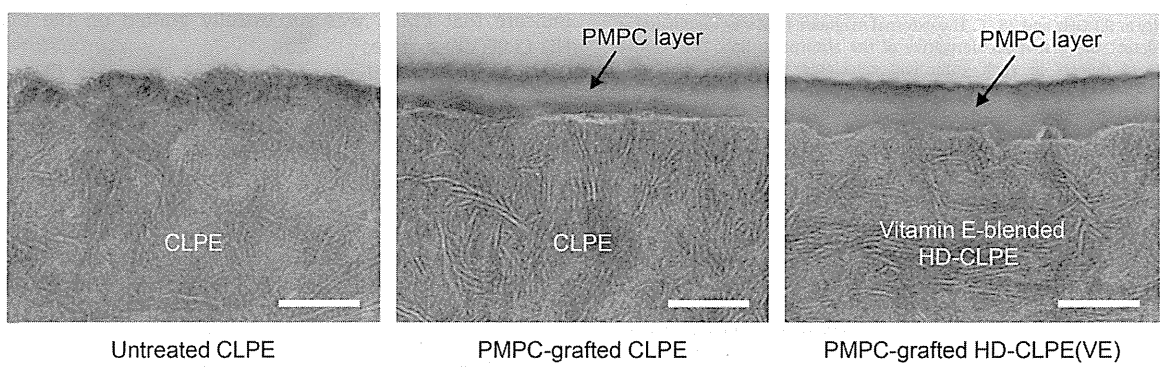

Fig. 2. Cross-sectional TEM images of untreated CLPE, PMPC-grafted CLPE, and PMPC-grafted HD-CLPE(VE) samples. The scale bar corresponds to 200 nm.

Table 1
Mechanical properties of untreated CLPE, PMPC-grafted CLPE, and PMPC-grafted HD-CLPE(VE).

Properties	Untreated CLPE (PE)	PMPC-grafted CLPE (PMPC-PE)	PMPC-grafted HD-CLPE(VE) (PMPC-VE)	Statistical analysis groups		
				PE vs PMPC-PE	PE vs PMPC-VE	PMPC-PE vs PMPC-VE
Yield strength (MPa)	22.6 (0.3)[a]	23.0 (0.3)	24.6 (0.2)	<0.05	<0.01	<0.01
Ultimate strength (MPa)	54.4 (3.8)	52.8 (2.1)	55.3 (3.9)	N.S.[b]	N.S.	N.S.
Elongation (%)	346.0 (18.1)	351.6 (35.6)	317.0 (16.2)	N.S.	<0.05	<0.05
Impact strength (kJ/m^2)	101.4 (5.6)	100.5 (0.8)	93.0 (1.1)	N.S.	<0.01	<0.01
Hardness (shore D)	66.8 (0.4)	66.8 (0.3)	66.6 (0.8)	N.S.	N.S.	N.S.
Creep deformation (%)	0.73 (0.07)	0.72 (0.06)	0.68 (0.06)	N.S.	N.S.	N.S.

[a] The standard deviations are shown in parentheses.
[b] N.S. indicates no statistical difference.

The vitamin E blending was found to affect the oxidation stability of CLPE by scavenging free radicals. As shown in Fig. 6A–B, all CLPE samples before gamma-ray sterilization contained slightly detectable free radicals that had not been completely eliminated. Multiple peaks corresponding to the alkyl or allyl radicals were observed in all samples after gamma-ray sterilization (Fig. 6C) [27]. The small detectable peaks corresponding to the tocopheroxyl radical (α-TO•) were observed only in the PMPC-grafted HD-CLPE(VE) samples. The residual free-radical concentration after gamma-ray sterilization did not differ significantly between all groups examined in this study (Fig. 6D). Interestingly, the oxidative-induction time of the PMPC-grafted HD-CLPE(VE) samples with residual free radicals was much longer than that of the untreated CLPE and PMPC-grafted CLPE samples (Fig. 7A). As a consequence, the oxidation index of the PMPC-grafted HD-CLPE(VE) sample that was subjected to accelerated aging was much lower (almost zero) than that of the untreated CLPE and PMPC-grafted CLPE samples (Fig. 7B). There was no significant difference in both oxidative-induction time and oxidation index between the untreated CLPE and PMPC-grafted CLPE samples, regardless of residual free-radical concentration.

4. Discussion

In this study, we demonstrated the fabrication of a highly hydrophilic and lubricious nanometer-scale modified surface by PMPC grafting onto the surface of an antioxidative CLPE substrate with vitamin E blending; we also investigated the effects of PMPC grafting and vitamin E blending on the wear resistance, oxidative stability, and mechanical properties of liners for artificial hip joints. The results provide preliminary evidence that the surface and substrate modifications affected the extent of the wear resistance, oxidative stability, and the underlying mechanical properties of the acetabular liner. This suggests that the PMPC-grafted surface and vitamin E-blended substrate may be a promising approach to extending the longevity of THA artificial joints.

To ensure the *in vivo* long-term wear resistance and oxidative stability of the acetabular liners, we used the photoinduced-radical graft polymerization technique to create strong bonding between the CLPE substrate and the PMPC graft chain [10,19], and we used antioxidant vitamin E blending to scavenge the residual free radicals. It has been known that the presence of vitamin E in the PE substrate, which prevents oxidation degradation, reduces the cross-linking efficiency because of the establishment of competition between the vitamin E itself and the alkyl or allyl radicals in the reaction with the radicals produced by gamma-ray irradiation [24]. In general, increased cross-linking in the CLPE with an increase in gamma-ray irradiation dose degrades its mechanical properties, producing a trade-off between wear resistance and mechanical properties. It is desirable to reduce wear while maintaining the mechanical properties necessary for proper *in vivo* function. Therefore, we optimized the gamma-ray irradiation dose for sufficiently effective cross-links to simultaneously obtain wear resistance and mechanical properties; the

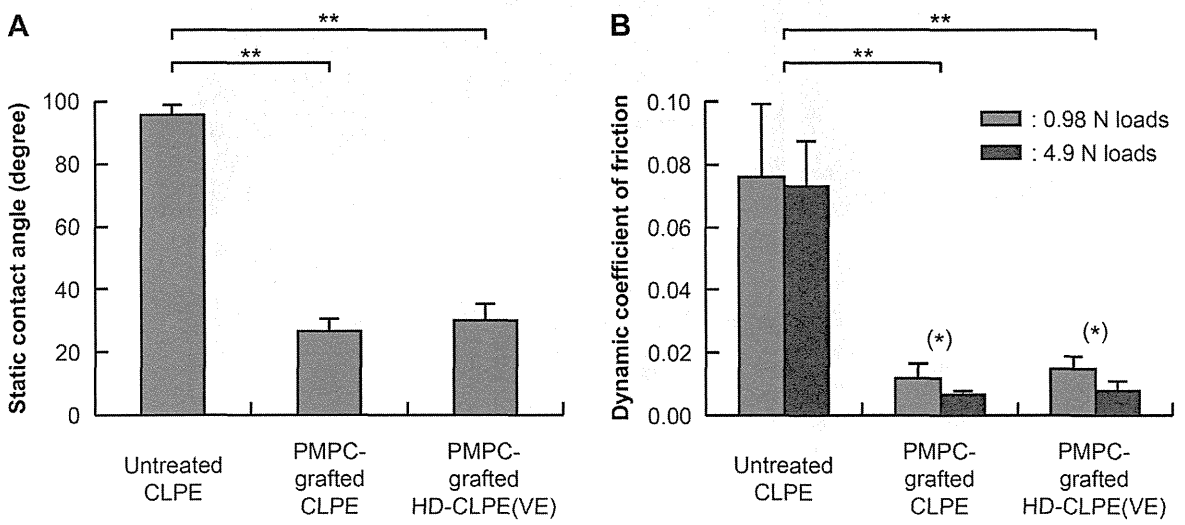

Fig. 3. (A) Static-water contact angle and (B) dynamic coefficient of friction of untreated CLPE, PMPC-grafted CLPE, and PMPC-grafted HD-CLPE(VE) samples. Data are expressed as means ± standard deviations. (*): *t*-Test, significant differences ($p < 0.05$) were observed in the comparison between 0.98 and 4.9 N loading groups, and **one-factor ANOVA and post-hoc test, significant difference ($p < 0.01$) were observed in the comparison between three groups of samples.

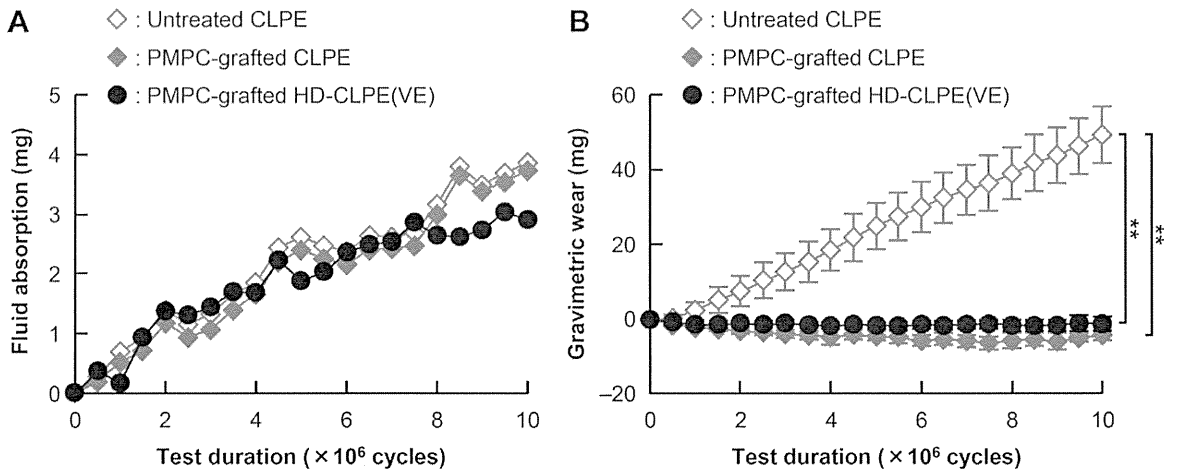

Fig. 4. Time course of (A) fluid absorption and (B) gravimetric wear of untreated CLPE, PMPC-grafted CLPE, and PMPC-grafted HD-CLPE(VE) liners during the hip-simulator wear test. Data are expressed as means ± standard deviations. **One-factor ANOVA and post-hoc test, significant differences ($p < 0.01$) were observed in the comparison of gravimetric wear after the test for all three groups of liners.

HD-CLPE(VE) was irradiated with a high-dose of 100-kGy gamma-rays in this study.

At the same time, there was concern that the presence of vitamin E on the CLPE surface reduced the PMPC-grafting efficiency because of the establishment of competition between the vitamin E and the semi-benzopinacol radicals in the benzophenone as a photoinitiator, in the reaction with photoinduced radicals. In Figs. 1 and 2, the results indicate that PMPC was successfully grafted on the CLPE and HD-CLPE(VE) surfaces independent of the presence of vitamin E [8,17,19,20]. The photoinduced-radical graft polymerization proceeded only on the surfaces of the CLPE and HD-CLPE(VE) substrates [16]. Therefore, surface cleanliness without fouling that involved an antioxidant was critical for the polymerization. The HD-CLPE(VE) of this study was fully washed with aqueous polysorbate-surfactant solutions and ethanol to completely remove vitamin E from the surface.

The bearing surfaces of a natural synovial joint are covered with a specialized type of hyaline cartilage, called articular cartilage, which protects the joint interface from mechanical wear and facilitates smooth motion of the joint during daily activities [20,28]. Articular cartilage consists of chondrocytes surrounded by extracellular matrix macromolecules (e.g., proteoglycans, glycosaminoglycans, and collagens) and surface active phospholipids (e.g., phosphatidylcholine derivatives). Owing to the charge on these molecules, they can trap water to maintain the water–fluid and electrolyte balance within the articular cartilage tissue, making it highly hydrophilic and providing an effective boundary lubricant [20,29]. The fluid thin-film lubrication achieved by the presence of

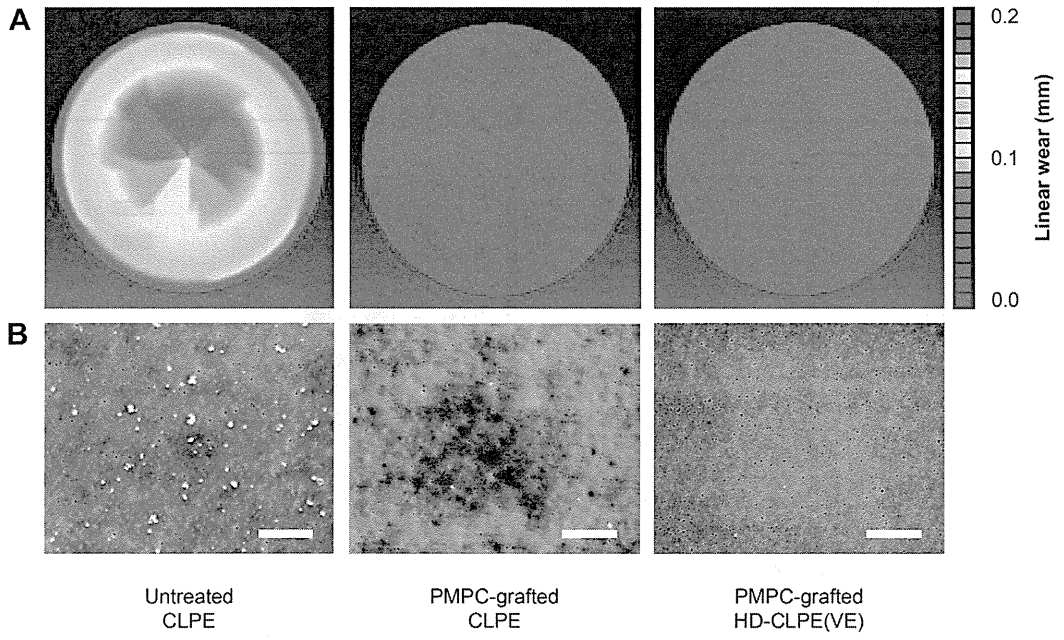

Fig. 5. Analyses of untreated CLPE, PMPC-grafted CLPE, and PMPC-grafted HD-CLPE(VE) liners after the hip-simulator wear test. (A) Three-dimensional coordinate measurements of various liners and (B) SEM images of wear particles isolated from lubricants of the hip-simulator wear test. The scale bar corresponds to 5 μm.

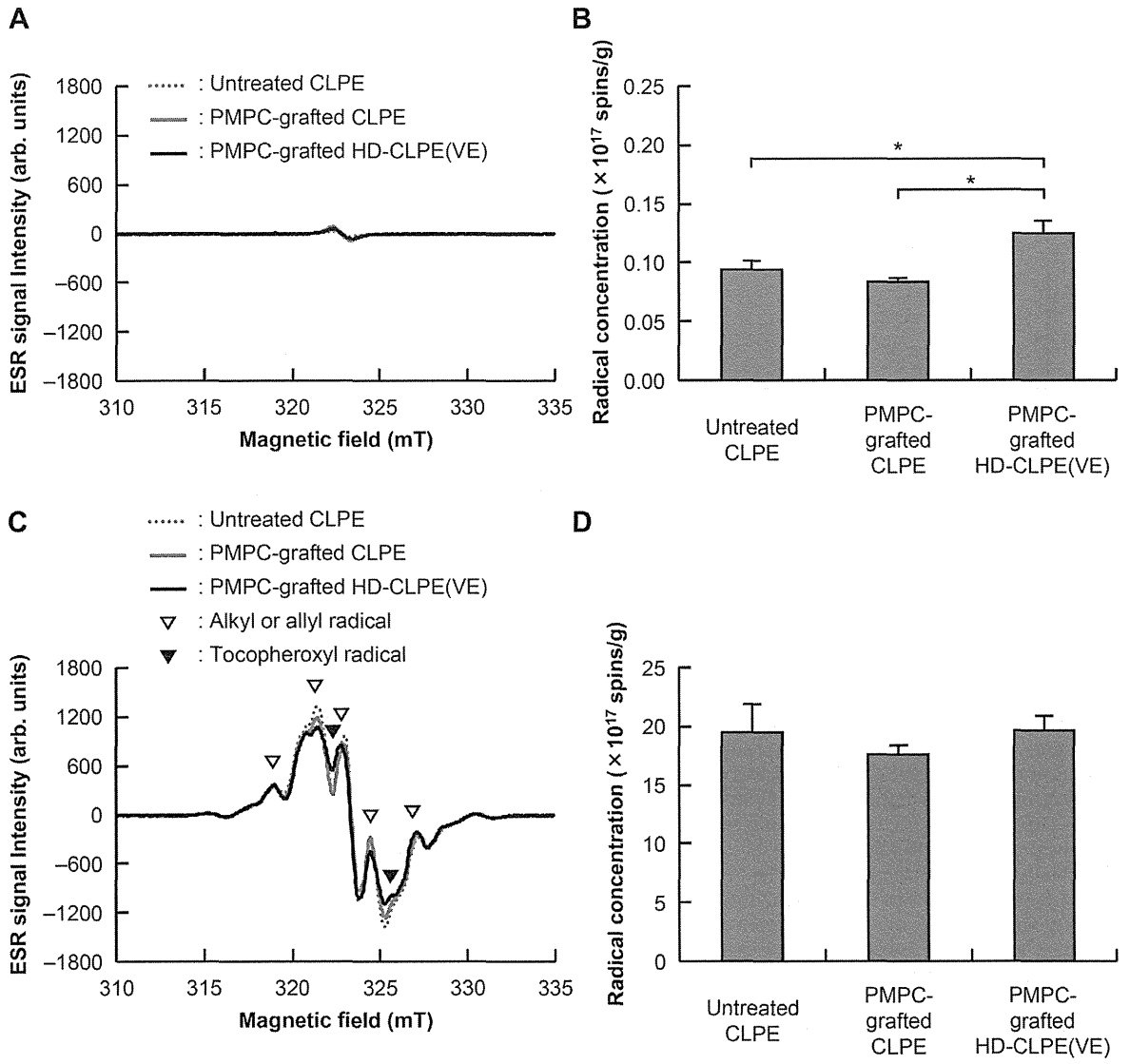

Fig. 6. Analyses of residual free radical of untreated CLPE, PMPC-grafted CLPE, and PMPC-grafted HD-CLPE(VE) samples. (A) ESR spectra and (B) residual free radical concentration before gamma-ray sterilization. (C) ESR spectra and (D) residual free radical concentration after gamma-ray sterilization. Data are expressed as means ± standard deviations. *One-factor ANOVA and post-hoc test, significant differences ($p < 0.05$) were observed in the comparison between all three groups of samples.

this hydrated layer is essential for the smooth motion of natural synovial joints.

The water wettabilities of the PMPC-grafted CLPE and PMPC-grafted HD-CLPE(VE) surfaces were found to be considerably greater than that of the untreated CLPE surfaces (Fig. 3A). This is caused by the presence of a nanometer-scale grafted PMPC layer that resulted from the polymerization of the highly hydrophilic MPC monomer. The fabrication of the PMPC gel layer clearly influenced the friction response; it can be observed in Fig. 3B that the dynamic coefficients of friction of the PMPC-grafted CLPE and PMPC-grafted HD-CLPE(VE) surfaces were significantly lower than those of the untreated CLPE surface. This is attributed to the significant increase in hydrophilicity evident from the reduction in the static-water contact angles on the PMPC-grafted surfaces [17]. Additionally, the improvement in the dynamic coefficients of friction of the PMPC-grafted CLPE and PMPC-grafted HD-CLPE(VE) surfaces in the case of 4.9 N loading compared with those in the case of 0.98 N loading is very interesting. These results show that the PMPC-grafted layer did not follow Amonton's law of $F = \mu N$. The contact stress of approximately 49 MPa at a load of 4.9 N, which was roughly calculated by the Hertzian theory, is higher than the tensile yield strength of the untreated CLPE, PMPC-grafted CLPE, and PMPC-grafted HD-CLPE(VE) (approximately 23–25 MPa in Table 1). The elastic CLPE and HD-CLPE(VE) substrates were slightly deformed by the loads, and the low friction coefficients may have been necessary to build a wider thin film of water over the larger contact area of the concave surfaces [19]. These results may also imply that the lubrication of PMPC-grafted CLPE and PMPC-grafted HD-CLPE(VE) was dominated by the hydration-lubrication mechanism [30]. Fortunately, the PMPC-grafted CLPE showed an extremely low and stable dynamic coefficient of friction in the case of large loads. The surface modification layer obtained by PMPC grafting was combined with the HD-CLPE(VE) substrate by strong C–C covalent bonding. Therefore, the obtained results support the motivation regarding PMPC grafting on the HD-CLPE(VE) surface. Additionally, it is thought that a sufficient number of strong bonds

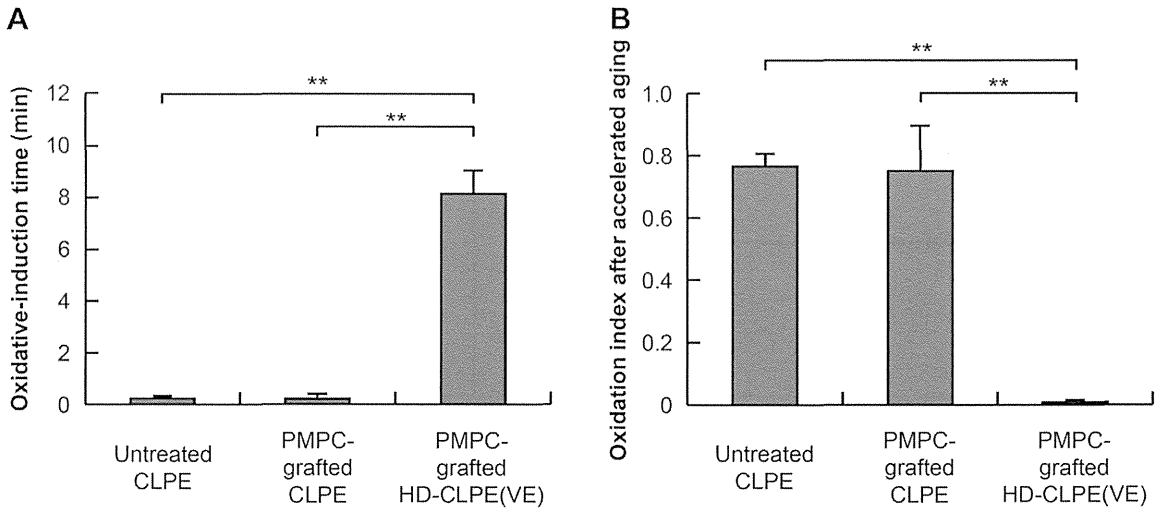

Fig. 7. Analyses of oxidative stability of untreated CLPE, PMPC-grafted CLPE, and PMPC-grafted HD-CLPE(VE) samples. (A) Oxidative-induction time and (B) oxidation index after accelerated aging. Data are expressed as means ± standard deviations. **One-factor ANOVA and post-hoc test, significant differences ($p < 0.01$) were observed in the comparison between all three groups of samples.

between the surface modification layer and the HD-CLPE(VE) surface are essential for the long-term retention of benefits of the grafted PMPC layer in artificial joints under variable and multidirectional loads [10].

In the hip-simulator wear test of the present study, the significant improvements observed in the water wettabilities and frictional properties of the PMPC-grafted CLPE and PMPC-grafted HD-CLPE(VE) liners resulted in substantial improvements in their wear resistances (Fig. 4B). The high friction of the untreated CLPE surfaces is one of their main disadvantages because it results in greater wear and possible seizure of bearing couples. The higher frictional properties of untreated CLPE surfaces were found to affect the wear properties, as determined by the hip-simulator wear test. In contrast, as noted earlier, the water wettabilities of the PMPC-grafted CLPE and PMPC-grafted HD-CLPE(VE) surfaces were considerably greater. Fluid-film lubrication (or hydration lubrication) of the PMPC-grafted surface was therefore provided by the hydrated layer. The obtained results confirm that orthopedic bearings using PMPC are able to mimic the natural articular cartilage that protects the joint interface from mechanical wear and facilitates smooth movement of the joints during daily activities [28,31]. The PMPC structure attracts water in a way that is similar to that of the extracellular matrix molecules present in cartilage, providing a lubricating layer on the surface to which they are attached [29]. The hydrophilic PMPC layer grafted onto the CLPE surface significantly increased lubrication to levels that match articular cartilage [32,33]. By mimicking the properties of the extracellular matrix of cartilage, the high wear resistance of the native tissue could be replicated by the use of an artificial polymer. Learning from and mimicking natural structures and systems have been shown to be a highly successful and advantageous approach to producing artificial tissues and implants. In particular, this study has demonstrated that investigating and subsequently mimicking natural structures and systems; the strategy of investigating and then reproducing the natural bearing surfaces in artificial joints to mimic the role of cartilage has great potential.

The production of wear particles in THA is recognized as the main factor behind the initiation of periprosthetic osteolysis and aseptic loosening [2,3]. The inflammatory cellular response to particles is thought to be dependent upon factors such as particle number, size, shape, surface area, and material chemistry [34]. If nanometer-scale particles are produced *in vivo*, it would be important to determine their biological activity relative to that of the micrometer-scale particles. In the wear particle analysis carried out in the present study, the wear particles collected from the PMPC-grafted CLPE and PMPC-grafted HD-CLPE(VE) liners were on the scale of sub-micrometers, regardless of PMPC grafting and vitamin E blending (Fig. 5B). Based on these results, we expect the *in vivo* biological response of the PMPC-grafted CLPE liners to be comparable with that of conventional, untreated CLPE [5]. Compared to particles generated by the lubricants used for the untreated liners, the remarkably smaller number of wear particles isolated from the lubricants used for the PMPC-grafted liners may help predict whether abnormal wear would occur. Moreover, several previous studies reported that vitamin E and wear particles containing vitamin E can possibly reduce the inflammatory cellular responses [35]. However, owing to the relatively short history of these materials, continuous attention must be paid to the submicrometer-size and number of abnormal wear particles in the PMPC-grafted CLPE and HD-CLPE(VE) liners, respectively.

Oxidation is primarily caused by the residual free radicals that are trapped in the crystalline phase of PE after gamma-ray irradiation. Therefore, post-irradiation thermal treatment has been used to reduce or eliminate those residual free radicals. One thermal-treatment process is annealing at a temperature below the melting point of PE (approximately 138 °C). In this process, the crystalline phase is partially melted, and the free radicals are reduced but not completely eliminated. As shown in Fig. 6A–B, all CLPE samples obtained in this study with annealing at 120 °C in N_2 gas contained slightly detectable free radicals. Another thermal-treatment process is melting at a temperature above 150 °C. Using this process, the number of residual free radicals is reduced until they are completely eliminated. On the other hand, the crystallinity is reduced after post-irradiation melting owing to the hindrance created by the newly formed cross-linking; the resulting mechanical properties including fatigue are reduced [36]. The retention of the bulk properties of the substrates is extremely important in clinical applications because the biomaterials used as implants act not only as surface-functional materials, but also as structural materials *in vivo*. For example, dislocation is the biggest short-term problem associated with THA [3]. A thin acetabular liner against a large femoral head not only allows for an increased

head/neck ratio, which is directly related to the range of motion prior to impingement of the trunnion on the liner, but also increases the jump distance. Hence, the use of implants with such dimensions is becoming more common in order to improve the stability of the bearing surface. Mechanical fracture attributed to scission of the PE molecular backbone owing to oxidation degradation in thin acetabular liners by the possible impingements must therefore be monitored. Several previous studies reported that the mechanical fracture was caused by neck impingements in the CLPE liners that were thermally treated via melting [37]. Among the data gathered to date for over 12,000 clinical applications of PMPC-grafted CLPE liner (Aquala® liner; KYOCERA Medical Corporation) that were thermally treated via annealing, we have observed neither mechanical fracture nor complication during follow-up assessment periods that spanned a minimum of 5 years and a maximum of 7 years. Therefore, we think that annealing as the post-irradiation thermal treatment has an advantage from the view point of mechanical properties. In reality, as shown in Table 1, all CLPE samples in this study maintained high level of mechanical properties as *in vivo* structural materials. Furthermore, the mechanical properties of the PMPC-grafted HD-CLPE(VE) samples remained almost unchanged even after vitamin E blending and PMPC grafting. This indicates that the diffusion of vitamin E during blending proceeded only in the amorphous phase of PE, primarily around the PE grain boundary [38], and photoinduced-radical graft polymerization occurred only on the surface of the substrates, whereas the properties of the substrates remained unchanged.

Moreover, it was recently reported that *in vivo* oxidation occurred, not only for the CLPE liner obtained after annealing, but also for the CLPE liner that was treated via melting [22]. In fact, the clinical impact of this oxidation degradation remains unclear. Although its clinical significance is still the subject of scientific debate, *in vivo* oxidation is regarded as undesirable. It is thought that the stabilization of the residual free radicals with an antioxidant such as vitamin E is necessary as an additional or alternative process. In Figs. 6 and 7, the PMPC-grafted HD-CLPE(VE) samples exhibited extremely high oxidative stability even though the amount of residual free radicals was at a detectable level. Despite the high-dose gamma-ray irradiation for cross-linking and further UV irradiation for PMPC grafting, the CLPE substrate modified by vitamin E blending maintained high resistance to oxidation. Indeed, vitamin E is an extremely efficient radical scavenger. The PMPC-grafted HD-CLPE(VE) samples contained 0.1 mass% of vitamin E; it was thought that the concentration of vitamin E was sufficient to obtain high oxidative stability even after cross-linking and PMPC grafting.

Despite these promising results, our study has a number of limitations. First, *in vitro* findings do not always translate to clinical success. We conducted clinical trials of PMPC-grafted CLPE liners at multiple medical centers between 2007 and 2009 in Japan [9]. Based on other related evidence and these clinical trials, the Japanese government (Ministry of Health, Labor, and Welfare, Japan) approved the clinical use of PMPC-grafted CLPE acetabular liners in artificial hip joints in April 2011. We observed neither osteolysis nor a need for revision surgery during follow-up periods of up to 7 years for the clinical trials. Second, we did not completely capture the range of loading and motion conditions of the *in vivo* environment in terms of the variety of positions during the hip-simulator wear test, the magnitude of loading, or the subjects' daily routine; however, in accordance with ISO 14242-3, we believe that these results can provide a good indication of wear performance. Third, as previously reported [34], the procedure for the isolation of wear particles in this study could not capture wear particles with a diameter below 0.1 μm. The cellular response to particles is thought to be dependent upon factors such as particle number, size, shape, surface area, and material chemistry. If nanometer-scale particles are generated *in vivo*, it will be important to determine their biological activity in relation to that of micrometer-scaled particles. Fourth, the wear performance we report is only valid for this specific combination of Co–Cr–Mo alloy femoral head with a diameter of 26 mm and PMPC-grafted HD-CLPE(VE) liner. Although aseptic loosening is one of the most common reasons for late-term revision surgery, dislocation is the biggest short-term problem [3]. A large femoral head not only allows for an increased head/neck ratio, which is directly related to the range of motion prior to impingement of the trunnion on the liner, but also increases the jump distance. Hence, larger femoral heads have recently come into more frequent use to improve the stability of the bearing surface. We believe that this drawback is partially offset by the long duration of the simulation. We are now running the hip-simulator wear tests using larger (i.e., 32–44 mm) Co–Cr–Mo alloy and zirconia-toughened alumina ceramic femoral heads and thin acetabular liners.

5. Conclusions

We have demonstrated that the PMPC grafting layer was successfully fabricated on the surface of an antioxidative vitamin E-blended CLPE substrate. The PMPC-grafted HD-CLPE(VE) provided high wear resistance, oxidative stability, and mechanical properties simultaneously. Since MPC is a highly hydrophilic compound, the water wettability and lubricity of the PMPC-grafted CLPE and HD-CLPE(VE) surfaces were greater than those of the untreated CLPE surface because of the formation of a PMPC grafting layer and its hydration, which can serve as an extremely efficient lubricant. It was also observed that the PMPC grafting significantly contributed to wear reduction. Despite the high-dose gamma-ray irradiation for cross-linking and further UV irradiation for PMPC grafting, the substrate modified by vitamin E blending maintained high oxidative stability because vitamin E is an extremely efficient radical scavenger. Furthermore, the results clearly showed that the mechanical properties of the substrate were minimally changed, if at all, even after PMPC grafting or vitamin E blending, or both PMPC grafting and vitamin E blending.

Acknowledgments

Part of this research was supported by Health and Welfare Research Grants for Research on Medical Devices for Improving Impaired QOL (H20-004) and Research on Measures for Intractable Diseases (H24-001) from the Japanese Ministry of Health, Labour and Welfare. The ESR analysis was conducted at the Research Hub for Advanced Nano Characterization, The University of Tokyo, supported by the Japanese Ministry of Education, Culture, Sports, Science and Technology. We thank Dr. Fumiaki Miyaji and Mr. Kenichi Saiga of KYOCERA Medical Corporation for their technical assistance.

References

[1] Kurtz S, Mowat F, Ong K, Chan N, Lau E, Halpern M. Prevalence of primary and revision total hip and knee arthroplasty in the United States from 1990 through 2002. J Bone Joint Surg Am 2005;87:1487–97.
[2] Harris WH. The problem is osteolysis. Clin Orthop Relat Res 1995;311:46–53.
[3] Bozic KJ, Kurtz SM, Lau E, Ong K, Vail TP, Berry DJ. The epidemiology of revision total hip arthroplasty in the United States. J Bone Joint Surg Am 2009;91(1):128–33.
[4] Jacobs JJ, Roebuck KA, Archibeck M, Hallab NJ, Glant TT. Osteolysis: basic science. Clin Orthop Relat Res 2001;393:71–7.
[5] Moro T, Takatori Y, Ishihara K, Konno T, Takigawa Y, Matsushita T, et al. Surface grafting of artificial joints with a biocompatible polymer for preventing periprosthetic osteolysis. Nat Mater 2004;3:829–37.

[6] Moro T, Takatori Y, Ishihara K, Nakamura K, Kawaguchi H. 2006 Frank Stinchfield Award: grafting of biocompatible polymer for longevity of artificial hip joints. Clin Orthop Relat Res 2006;453:58–63.
[7] Moro T, Kawaguchi H, Ishihara K, Kyomoto M, Karita T, Ito H, et al. Wear resistance of artificial hip joints with poly(2-methacryloyloxyethyl phosphorylcholine) grafted polyethylene: comparisons with the effect of polyethylene cross-linking and ceramic femoral heads. Biomaterials 2009;30(16):2995–3001.
[8] Kyomoto M, Moro T, Takatori Y, Kawaguchi H, Ishihara K. Cartilage-mimicking, high-density brush structure improves wear resistance of crosslinked polyethylene: a pilot study. Clin Orthop Relat Res 2011;469(8):2327–36.
[9] Takatori Y, Moro T, Kamogawa M, Oda H, Morimoto S, Umeyama T, et al. Poly(2-methacryloyloxyethyl phosphorylcholine)-grafted highly cross-linked polyethylene liner in primary total hip replacement: one-year results of a prospective cohort study. J Artif Organs 2013;16(2):170–5.
[10] Moro T, Takatori Y, Kyomoto M, Ishihara K, Hashimoto M, Ito H, et al. Long-term hip simulator testing of the artificial hip joint bearing surface grafted with biocompatible phospholipid polymer. J Orthop Res 2014;32(3):369–76.
[11] Iwasaki Y, Ishihara K. Cell membrane-inspired phospholipid polymers for developing medical devices with excellent biointerfaces. Sci Technol Adv Mater 2012;13:064101 [p. 14].
[12] Kuiper KK, Nordrehaug JE. Early mobilization after protamine reversal of heparin following implantation of phosphorylcholine-coated stents in totally occluded coronary arteries. Am J Cardiol 2000;85:698–702.
[13] Selan L, Palma S, Scoarughi GL, Papa R, Veeh R, Di Clemente D, et al. Phosphorylcholine impairs susceptibility to biofilm formation of hydrogel contact lenses. Am J Ophthalmol 2009;147:134–9.
[14] Snyder TA, Tsukui H, Kihara S, Akimoto T, Litwak KN, Kameneva MV, et al. Preclinical biocompatibility assessment of the EVAHEART ventricular assist device: coating comparison and platelet activation. J Biomed Mater Res A 2007;81(1):85–92.
[15] Kyomoto M, Moro T, Konno T, Takadama H, Yamawaki N, Kawaguchi H, et al. Enhanced wear resistance of modified cross-linked polyethylene by grafting with poly(2-methacryloyloxyethyl phosphorylcholine). J Biomed Mater Res A 2007;82(1):10–7.
[16] Kyomoto M, Moro T, Konno T, Takadama H, Kawaguchi H, Takatori Y, et al. Effects of photo-induced graft polymerization of 2-methacryloyloxyethyl phosphorylcholine on physical properties of cross-linked polyethylene in artificial hip joints. J Mater Sci Mater Med 2007;18:1809–15.
[17] Kyomoto M, Moro T, Miyaji F, Hashimoto M, Kawaguchi H, Takatori Y, et al. Effect of 2-methacryloyloxyethyl phosphorylcholine concentration on photo-induced graft polymerization of polyethylene in reducing the wear of orthopaedic bearing surface. J Biomed Mater Res A 2008;86(2):439–47.
[18] Kyomoto M, Moro T, Miyaji F, Konno T, Hashimoto M, Kawaguchi H, et al. Enhanced wear resistance of orthopaedic bearing due to the cross-linking of poly(MPC) graft chains induced by gamma-ray irradiation. J Biomed Mater Res B Appl Biomater 2008;84:320–7.
[19] Kyomoto M, Moro T, Miyaji F, Hashimoto M, Kawaguchi H, Takatori Y, et al. Effects of mobility/immobility of surface modification by 2-methacryloyloxyethyl phosphorylcholine polymer on the durability of polyethylene for artificial joints. J Biomed Mater Res A 2009;90(2):362–71.
[20] Kyomoto M, Moro T, Saiga K, Hashimoto M, Ito H, Kawaguchi H, et al. Biomimetic hydration lubrication with various polyelectrolyte layers on cross-linked polyethylene orthopedic bearing materials. Biomaterials 2012;33(18):4451–9.
[21] Currier BH, Currier JH, Mayor MB, Lyford KA, Collier JP, Van Citters DW. Evaluation of oxidation and fatigue damage of retrieved crossfire polyethylene acetabular cups. J Bone Joint Surg Am 2007;89(9):2023–9.
[22] MacDonald D, Sakona A, Ianuzzi A, Rimnac CM, Kurtz SM. Do first-generation highly crosslinked polyethylenes oxidize in vivo? Clin Orthop Relat Res 2011;469(8):2278–85.
[23] Bracco P, Oral E. Vitamin E-stabilized UHMWPE for total joint implants: a review. Clin Orthop Relat Res 2011;469(8):2286–93.
[24] Oral E, Godleski Beckos C, Malhi AS, Muratoglu OK. The effects of high dose irradiation on the cross-linking of vitamin E-blended ultrahigh molecular weight polyethylene. Biomaterials 2008;29(26):3557–60.
[25] Ishihara K, Ueda T, Nakabayashi N. Preparation of phospholipid polymers and their properties as polymer hydrogel membranes. Polym J 1990;22(5):355–60.
[26] Kurtz SM, Muratoglu OK, Buchanan F, Currier B, Gsell R, Greer K, et al. Interlaboratory reproducibility of standard accelerated aging methods for oxidation of UHMWPE. Biomaterials 2001;22(13):1731–7.
[27] Ridley MD, Jahan MS. Effects of packaging environments on free radicals in gamma-irradiated UHMWPE resin powder blend with vitamin E. J Biomed Mater Res A 2009;88(4):1097–103.
[28] Kirk TB, Wilson AS, Stachowiak GW. The morphology and composition of the superficial zone of mammalian articular cartilage. J Orthop Rheumatol 1993;6:21–8.
[29] Goldberg R, Schroeder A, Silbert G, Turjeman K, Barenholz Y, Klein J. Boundary lubricants with exceptionally low friction coefficients based on 2D close-packed phosphatidylcholine liposomes. Adv Mater 2011;23:3517–21.
[30] Ishikawa Y, Hiratsuka K, Sasada T. Role of water in the lubrication of hydrogel. Wear 2006;261:500–4.
[31] Bhosale AM, Richardson JB. Articular cartilage: structure, injuries and review of management. Br Med Bull 2008;87:77–95.
[32] Raviv U, Glasson S, Kampf N, Gohy JF, Jérôme R, Klein J. Lubrication by charged polymers. Nature 2003;425:163–5.
[33] Chen M, Briscoe WH, Armes SP, Klein J. Lubrication at physiological pressures by polyzwitterionic brushes. Science 2009;323(5922):1698–701.
[34] Tipper JL, Galvin AL, Williams S, McEwen HM, Stone MH, Ingham E, et al. Isolation and characterization of UHMWPE wear particles down to ten nanometers in size from in vitro hip and knee joint simulators. J Biomed Mater Res A 2006;78(3):473–80.
[35] Bladen CL, Teramura S, Russell SL, Fujiwara K, Fisher J, Ingham E, et al. Analysis of wear, wear particles, and reduced inflammatory potential of vitamin E ultrahigh-molecular-weight polyethylene for use in total joint replacement. J Biomed Mater Res B Appl Biomater 2013;101(3):458–66.
[36] Oral E, Malhi AS, Muratoglu OK. Mechanisms of decrease in fatigue crack propagation resistance in irradiated and melted UHMWPE. Biomaterials 2006;27(6):917–25.
[37] Ast MP, John TK, Labbisiere A, Robador N, Valle AG. Fractures of a single design of highly cross-linked polyethylene acetabular liners: an analysis of voluntary reports to the United States Food and Drug Administration. J Arthroplasty; in press.
[38] Shibata N, Tomita N. The anti-oxidative properties of alpha-tocopherol in gamma-irradiated UHMWPE with respect to fatigue and oxidation resistance. Biomaterials 2005;26(29):5755–62.

Sugita et al. BMC Musculoskeletal Disorders 2014, 15:203
http://www.biomedcentral.com/1471-2474/15/203

BMC Musculoskeletal Disorders

RESEARCH ARTICLE Open Access

Clinical characteristics of rheumatoid arthritis patients undergoing cervical spine surgery: an analysis of National Database of Rheumatic Diseases in Japan

Shurei Sugita[1*], Hirotaka Chikuda[1], Yuho Kadono[1], Hiroshi Ohtsu[2], Katsushi Takeshita[1], Jinju Nishino[3], Shigeto Tohma[4] and Sakae Tanaka[1]

Abstract

Background: The aim of this study was to examine the clinical characteristics of rheumatoid arthritis (RA) patients who underwent cervical spine surgery using a multicenter observational database.

Methods: We obtained data from a nationwide observational cohort database of patients with rheumatic diseases (National Database of Rheumatic Diseases by iR-net in Japan (NinJa)) for the fiscal years 2003 to 2011. A total of 39 out of 60 patients who underwent cervical spine surgery for a RA-related cause and whose data were available for two consecutive years (to assess the preoperative patient status) were chosen as cases. Patients with a non-RA-related cause of surgery (e.g., trauma) were excluded. First, we compared the patient characteristics between the cases and total patients in the same fiscal year. Next, 106 eligible controls, who were defined as RA patients enrolled in the same fiscal year as the case subjects, who were matched for age, gender and disease duration (within ±1 year), were selected. We compared the demographic data between the two groups. We also calculated the percentage of patients who underwent cervical spine surgery (surgeries/total number of patients) in fiscal years 2003 to 2011.

Results: Although the proportion of patients using biologics linearly increased during study period, the percentage of patients undergoing cervical spine surgeries remained unchanged, at approximately 0.15%. These cases had more tender joints (3 vs. 1, $p < 0.01$) and exhibited a significantly higher Modified Health Assessment Questionnaire (MHAQ) score (1.13 vs. 0.5, $p < 0.01$), C-reactive protein (CRP) (1.5 vs. 0.36, $p < 0.01$), and disease activity score (DAS) 28-CRP (3.63 vs. 2.81, $p < 0.01$) compared to the controls.

Conclusions: Our study revealed that RA patients requiring cervical spine surgery have a higher disease activity (as represented by the DAS28-CRP) and are more functionally disabled (as represented by the MHAQ) than control patients.

Keywords: Rheumatoid arthritis, Cervical spine surgery, Database

Background

Rheumatoid arthritis (RA) is a chronic inflammatory disease that affects the synovial joints. Immunologic dysfunction results in the hypertrophy of the synovial tissue, causing erosion of the articular cartilage and subchondral bone [1]. The involvement of the cervical spine is common in RA patients, with a reported prevalence of up to 86% [2]. The majority of RA patients with radiological abnormalities of the cervical spine remain asymptomatic for years [3]. Only a small fraction of patients eventually require surgical treatment, primarily due to neurological deterioration. For those who need surgical intervention, early surgical intervention is desirable [2,4]. If there is a delay in surgical intervention, it can lead to a poor outcome and even death [5,6]. Neurological improvement can be seen after surgery; in one study, patients with

* Correspondence: ssugita-tky@umin.ac.jp
[1]The Department of Orthopaedic Surgery, The University of Tokyo, Hongo 7-3-1, Bunkyo, Tokyo, Japan
Full list of author information is available at the end of the article

RA and patients with osteoarthritis had similarly high proportions of good global scores and satisfaction with their treatment after surgery [7]. However, it remains unclear whether RA patients undergoing cervical spine surgery differ from those who do not receive surgical treatment in terms of their clinical characteristics and the disease activity of RA. A previous cohort study showed a correlation between the severity of the RA activity in the peripheral joints and the progression of cervical spine instability [8]. However, few studies using a large observational database have examined this issue.

The aim of this study was to examine the clinical characteristics of RA patients who underwent cervical spine surgery using a multicenter observational database. Our hypothesis is that RA patients requiring cervical spine surgery have a higher disease activity than those who do not undergo surgical treatment.

Methods

Data source

The National Database of Rheumatic Diseases by iR-net in Japan (NinJa) is a nationwide, multicenter (40 centers), observational cohort database of patients with rheumatic diseases established in 2002 in Japan [9]. The collected data consist of two components: patient information over the course of the year [outcome, death, hospitalization, operations, number of total joint arthroplasty procedures in large joints (hip, knee, shoulder, elbow), malignancy and tuberculosis] and information collected on each day that the patient visits the outpatient department of each center [tender-joint count (TJC) and swollen-joint count (SJC), modified health assessment questionnaire (MHAQ) score, Steinbrocker functional classification (class), patient global and pain visual analog scale scores (PtGVAS, PtPainVAS), the doctor VAS (DrGVAS), erythrocyte sedimentation rate (ESR), C-reactive protein (CRP) level, disease activity score (DAS) 28-CRP and the use of corticosteroids, methotrexate (MTX) or biologics].

Patients

The data of RA patients who were enrolled in the fiscal years from 2003 to 2011 were employed for the analysis (the fiscal year was defined as April to March, because official schedule tends to be run according to the fiscal year in Japan). The data acquired from 2002 was eliminated because of the incompleteness of data. All patients fulfilled the 1987 classification criteria of the American College of Rheumatology. After simple comparison of the demographic data year by year, the patients who underwent cervical spine surgery (excluding those who underwent cervical spine surgery for non-RA-related causes) and whose data were available for two consecutive years were chosen as cases. The total number of cases included was 39.

The background data of the cases were extracted from the fiscal year before surgery to represent the preoperative status. We first simply compared the background data of the patients between the cases and total patients enrolled in the same fiscal year. Then, eligible controls (1:3 pair matching) were selected, which were defined as patients enrolled in the same fiscal year as the case subjects, who were matched for age (within ±1 year), gender and disease duration (within ±1 year). The total number of controls was 106. Some cases did not have three controls. The background data of the cases in the previous year of surgery and the controls were compared. The examined factors were the stage, class, MHAQ, CRP, ESR, PtPainVAS, PtGVAS, DrGVAS, DAS28-CRP, number of arthroplasty procedures, tender-joint count and the use of steroids, MTX or biologics.

The NinJa project was reviewed and approved by the National Hospital Organization research ethics committees, and this study protocol was approved by the research ethics committees of the Sagamihara National Hospital and the University of Tokyo Hospital, and all enrolled patients provided their written informed consent.

Analyses and statistics

The JMP 11.0.0 software program (SAS, Cary, NC) was used for the statistical analysis. Descriptive statistics were used to analyze the clinical information, demographic factors and other test data. Continuous variables were expressed as the medians and interquartile ranges (IQR). Yearly trends were analyzed by a single regression model or chi-square test, or by the Tukey-Kramer method. Differences between groups were examined using the Mann–Whitney U test for continuous variables or the chi-square test for categorical data, when appropriate. A p-value <0.05 was considered to indicate a significant difference.

Results

Table 1 shows the demographic and disease characteristics of the patients included in the NinJa Database. There were no significant yearly differences in gender (chi-square test). However, the age was significantly older in 2010 ($p < 0.01$, Tukey-Kramer method) and the disease duration was significantly shorter in fiscal year 2007 ($p < 0.01$, Tukey-Kramer method) (Table 1). The proportion of patients using corticosteroids decreased from 2003 to 2011, whereas the proportion using MTX and biologics linearly increased during this period (coefficient: 2.43, $p < 0.01$ for MTX, coefficient 2.76, $p < 0.01$ for biologics, single regression model) (Table 1). We also counted the number of patients who underwent cervical spine surgery or total joint replacement and those with RA recruited in this database in each fiscal year. The annual incidence of cervical spine surgery was approximately 0.17%, and

Table 1 Demographic and desease characteristics of the patients included in NinJa database

Fiscal year	2003	2004	2005	2006	2007	2008	2009	2010	2011	p-value	Coefficient
Total number of registered patients	4100	3994	4650	5152	5463	6502	7179	7254	10368		
Age (years) (IQR)	62(55–69)	63(55–70)	64(56–71)	63(56–71)	64(56–71)	64(56–71)	64(56–72)	65(57–72)	65(56–72)	<0.0001	
Gender (female:male)	3410:700	3313:681	3832:818	4229:923	4448:1015	5346:1156	5895:1284	5921:1333	8375:1993	0.7341	
Disease dutaion (years) (IQR)	11(5–20)	11(5–19)	10(5–19)	10(5–19)	9(4–19)	10(5–19)	10(5–19)	10(5–19)	9(4–18)	0.0020	
Use of MTX (%)	36	48	53	53	47	51	64	58	60	0.0084	2.43
Use of corticosteroid (%)	64	63	62	63	61	58	53	53	49	0.0002	−1.88
Use of biologics (%)	0.4	2.1	4.3	9	12	14	20	19	20	<0.0001	2.76
Cervical spine surgery (cases) (%)	8 (0.19)	7 (0.17)	4 (0.08)	6 (0.12)	8 (0.15)	10 (0.15)	10 (0.14)	15 (0.21)	30 (0.29)	0.1593	0.01
Total knee replacement (cases) (%)	146 (3.55)	121 (3.02)	117 (2.52)	130 (2.52)	132 (2.42)	118 (1.81)	156 (2.17)	133 (1.87)	158 (1.52)	0.0002	−0.21
Total hip replacement (cases) (%)	33 (0.80)	37 (0.93)	50 (1.08)	48 (0.93)	45 (0.82)	51 (0.78)	46 (0.64)	43 (0.59)	56 (0.54)	0.0098	−0.05

The data are represented as the medians (IQR). The yearly differences were analyzed by the Tukey-Kramer method.
Yearly trends were analyzed by a single regression model, and are expressed by coefficients and p-values.

remained relatively stable during the study period, whereas that of total joint replacement showed a slightly decreasing trend (coefficient −0.21, $p < 0.01$ for total knee replacement, coefficient −0.05, $p < 0.01$ single regression model) (Table 1).

Fusion surgery was the most frequently performed surgery (29 cases, 74.4%), followed by laminoplasty (four cases, 10.25%), laminectomy (two cases, 5.1%) and unspecified surgery (four cases, 10.25%).

Table 2 summarizes the patient characteristics, which compared the cases and total patients enrolled in the same fiscal year. The data showed that the cases tended to be more functionally disabled (e.g. MHAQ, PtGVAS) and to have a more severe RA status (e.g. number of arthroplastic surgeries, tender joint count, swollen joint count, CRP, ESR, DAS28-CRP) and to have a longer disease duration. However, RA is known to be progressive disease, and there was a possibility that a longer disease duration could have influenced the other parameters (function, RA severity). Therefore, we decided to compare the characteristics of the patients using a case-matched study, as described in the Methods.

Table 3 summarizes the patient characteristics according to whether they underwent cervical spine surgery. The patients who underwent cervical spine surgery were more likely to have more tender joints (3 vs. 1, $p < 0.01$). They also exhibited significantly higher MHAQ scores (1.13 vs. 0.5, $p < 0.01$), higher DAS28-CRP values (3.63 vs. 2.81, $p < 0.01$), a higher PtGVAS (4.9 vs. 2.9, $p < 0.05$) and a higher DrGVAS (3.4 vs. 1.6, $p < 0.05$). They also tended to be in higher Steinbrocker functional classification ($p < 0.05$). Regarding the treatment of RA, the use of MTX was significantly lower in cases (13% vs. 40%, $p < 0.01$), and use of corticosteroids was significantly higher in cases (90% vs. 60%, $p < 0.01$) than controls. The use of biologics was not significantly different between cases and controls.

Discussion

In this retrospective analysis using a large database, we found that only a small fraction (1.7/1,000/year) of patients underwent cervical spine surgery. However, despite the increasing use of biologics, the incidence of cervical spine surgery remained unchanged over recent years. Our data also showed that patients undergoing cervical spine surgery had a higher disease activity and exhibited a more severe degree of functional disability than those who did not undergo cervical spine surgery.

Although radiographic abnormalities of the cervical spine are frequently seen in RA patients [2], our study showed that only a small fraction (1.7/1,000/year) of patients had a history of cervical spine surgery. A previous study showed that the number of RA-related cervical spinal surgeries in 609 RA patients was 0.2%, which was similar to our data [10]. There was a stark discrepancy between the high prevalence of radiographic abnormalities and the relative rarity of cervical spine surgery. There are several possible explanations for this discrepancy. One is that the prognosis of RA patients with cervical lesions is generally favorable. For example, a previous report showed that there was cervical spine involvement in up to 86% of RA patients, but only 10% of these patients actually developed neurological deterioration [11]. However, it is also possible that some patients were underdiagnosed, presumably due to the involvement of multiple joints.

The annual incidence of cervical spine surgery did not change much during recent years according to the NinJa database. The increased use of biologics has reportedly led to a reduction in the number of RA-related arthroplasty procedures, such as total hip replacements [12]. Our data agreed with this previous study, showing a decrease in the number of total joint replacement surgeries; however, the number of cervical spine surgeries did not exhibit a substantial decrease. We hypothesize that the protective effects of biologics on the cervical spine are limited. In line with this view, a prior study showed that the use of biologics prevented the development of de novo cervical spine lesions in RA patients, but failed to inhibit the progression of preexisting RA lesions [13]. Regarding the use of MTX, our data showed that the use of MTX was significantly lower in cases than controls. Another previous study showed that the use of MTX did not improve the cervical spine instability [14], so our results are reasonable. On the contrary, the use of corticosteroids was significantly higher in cases than in controls. A previous study showed that the administration of a higher dose of corticosteroid was a significant general factor predicting the development of myelopathy [15], supporting our present findings.

We also found that patients undergoing cervical spine surgery had a high disease activity despite receiving intensive treatment for RA, including biologics. There was a previous study that showed a correlation between the progression of peripheral erosive disease and the severity of cervical subluxation [16]. Our data further supported that study by using a case-matched method. Some previous reports recommended early prophylactic surgical intervention for cervical instability in RA patients [17-19]. Regardless whether surgery is undertaken, patients with a high disease activity should be closely monitored for neurological deterioration.

Interestingly, there were no significant differences in the pain scores between those with and without a history of cervical spine surgery. Therefore, physicians should pay close attention to not only the patient's pain, but also the neurological status and function of patients who do not report high pain levels.